THE UNIVERSITY OF ALBERTA

PARTICLE DYNAMICS IN A MICROPARTICLE LINEAR ACCELERATOR

by

© SAKTIBILASH PRAMANIK

A THESIS

SUBMITTED TO THE FACULTY OF GRADUATE STUDIES

IN PARTIAL FULFILMENT OF THE REQUIREMENTS

FOR THE DEGREE OF MASTER OF SCIENCE

DEPARTMENT OF ELECTRICAL ENGINEERING

EDMONTON, ALBERTA

FALL, 1969

Thesis 1977F 197

UNIVERSITY OF ALBERTA

FACULTY OF GRADUATE STUDIES

The undersigned certify that they have read, and recommend to the Faculty of Graduate Studies for acceptance, a thesis entitled Particle Dynamics in a Microparticle Linear Accelerator submitted by Saktibilash Pramanik in partial fulfilment of the requirements for the degree of Master of Science.

ABSTRACT

An analytical and numerical study is made of a low frequency Sloan-Lawrence structure with electrostatic quadrupoles within the drift tubes for accelerating charged microparticles. An improved set of equations has been derived to study the dynamics of the charged particles. These equations have been used to arrive at several structure designs, and these structures in turn have been examined for angular acceptance, phase acceptance, and acceptance in charge to mass ratios. The ranges of operating frequencies and charge to mass ratios considered are 30-50 KHz and 26-84 coulombs/kg respectively.

ACKNOWLEDGEMENT

The author gratefully acknowledges the encouragement and guidance received from the supervising professor, Dr. F. E. Vermeulen throughout the course of this research.

The author wishes to express his indebtedness to the National Research Council and The Department of Electrical Engineering for the award of a Teaching Assistantship.

The author also owes a debt of gratitude to his parents for their good wishes.

[illegible]

[illegible]

[illegible]

[illegible]

TABLE OF CONTENTS

LIST OF ILLUSTRATIONS

LIST OF TABLES

CHAPTER 1

INTRODUCTION

This thesis deals with a study of a low frequency Sloan-Lawrence structure for the acceleration of electrically charged microparticles for the simulation of micrometeoroids. The structure consists of a series of cylindrical drift tubes and accelerating gaps. In this type of structure axial particle stability is incompatible with simultaneous radial particle stability. To overcome this difficulty and to provide stability in both axial and radial directions the effect of auxiliary focusing elements in the structure is examined.

In principle there are various kinds of focusing arrangements which can be used, such as solenoid focusing, quadrupole focusing and self focusing. Of all the recently developed focusing systems, quadrupole focusing is the most efficient and it is the type of focusing studied in this work.

The idea of using quadrupole magnets as focusing elements was first introduced by E. D. Courant et al[(1)], during an investigation of the feasibility of alternating gradient synchrotrons. In 1941 D. W. Kerst and R. Serber[(2)], found that in the induction accelerator the strength of the focusing force is limited by the stability criterion: $0<n<1$, where n is called the field index and is given by the expression $n = -\left(\frac{r}{B}\right)\left(\frac{dB}{dr}\right)$, r is the radial displacement and B is the magnetic field. If n is much greater that 1 (rapid decrease of field strength in the radial direction), a strong focusing field

[illegible]

results in the vertical plane (refer to fig. 1-1) while the radial motion is strongly defocused. If the next section has a large negative n (rapid increase of field in the radial direction) there will be a strong radial focusing force with a large defocusing force in the vertical plane. In 1951 E. D. Courant et al showed that the net effect of these two

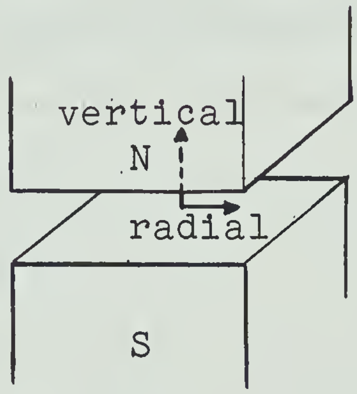

Fig. 1-1 Section of Induction Accelerator

sections is convergent in both the vertical and the horizontal planes to a greater extent than in a constant gradient magnetic field with a value of n lying between 0 and 1.

In the same year J. P. Blewett[3] showed that the same type of alternating gradient focusing quadrupoles can effectively be used for linear particle accelerators of the Alvarez type. His lens system consisted of quadrupole magnets placed axially inside the drift tubes of the accelerator such that in alternate drift tubes the quadrupoles are rotated through 90 degrees about the axis of the accelerator. The gradual development of this work in chronological order is listed in the references by 1, 3 to 12, and 14.

This work consists of three main chapters. The first of these, Chapter 2, deals in detail with the equations of motion of a particle in the accelerating structure. A series of equations to describe the particle dynamics is derived. These equations are more accurate and general than those used by previous workers[2,6,7,8,14].

Chapter 3 consists of an analytic study of transverse particle motion in a long accelerator structure under the simplifying assumptions that the particle velocity remains constant and that the structure is periodic. Analytical expressions have been derived for the transverse excursions of a particle at the injection plane and at all succeeding transverse planes at the middle of the drift tubes. A general expression for the acceptance in phase space has been derived in any of the above planes along the accelerator.

In Chapter 4 a numerical study of the behavior of various structures is made using the equations derived in Chapter 2. The results of this study are presented in tabular and graphical forms.

CHAPTER 2

PARTICLE DYNAMICS IN A MICROPARTICLE LINEAR ACCELERATOR

2.1 Radial Motion in the Accelerating Gap

2.1.1 General Equations and Assumptions

The equations of motion of the charged microparticle in the accelerating gap are derived from the Lorentz force equation:

$$\frac{d(m\bar{v})}{dt} = q(\bar{E}-\bar{v}x\bar{B}) \quad \text{------------------------------------(2-1)}$$

where t is the time

v is the velocity of the particle

q is the charge on the particle

$\bar{B}$ is the magnetic field intensity

$\bar{E}$ is the electric field intensity.

The velocity of the microparticles is very low and, therefore, the component of force due to magnetic field is neglected. It then follows from the foregoing equation that the radial motion of the particle is described by

$$m\ddot{r}-mr\dot{\theta}^2 = qE_r(r,Z)\ \mathrm{COS}(\omega t+\phi) \quad \text{----------------------------(2-2)}$$

where r is the radial excursion of the particle from the axis of the accelerator

E_r is the radial component of the electric field intensity

$\dot{\theta}$ is the angular velocity

z is the distance measured along the axis of the accelerator

ω is the operating frequency

ϕ is the phase difference between the instant in time at which the accelerating field reaches its peak value and the instant at which the particle crosses the electrical centre($Z=0$). ϕ is positive if the particle crosses the electrical centre after the field has reached its peak value. The exact definition of the electrical centre is given in Appendix 1. In this work, as in most other cases, the electrical centre is the mid-point of the gap.

The present study is restricted to an accelerator of the Sloan-Lawrence type. In this accelerator the reference particle or the so-called synchronous particle traverses the distance between two successive gap centres in exactly T/2, i.e., one half cycle of the applied electric field. As a consequence the synchronous particle traverses all the gaps while the fields are accelerating and is shielded in the drift tubes while the gap fields are decelerating. All quantities such as energy, velocity, phase, etc., associated with the synchronous particle are designated by the subscript 's'. Fig. 2.1 illustrates the principle of operation of a Sloan-Lawrence structure.

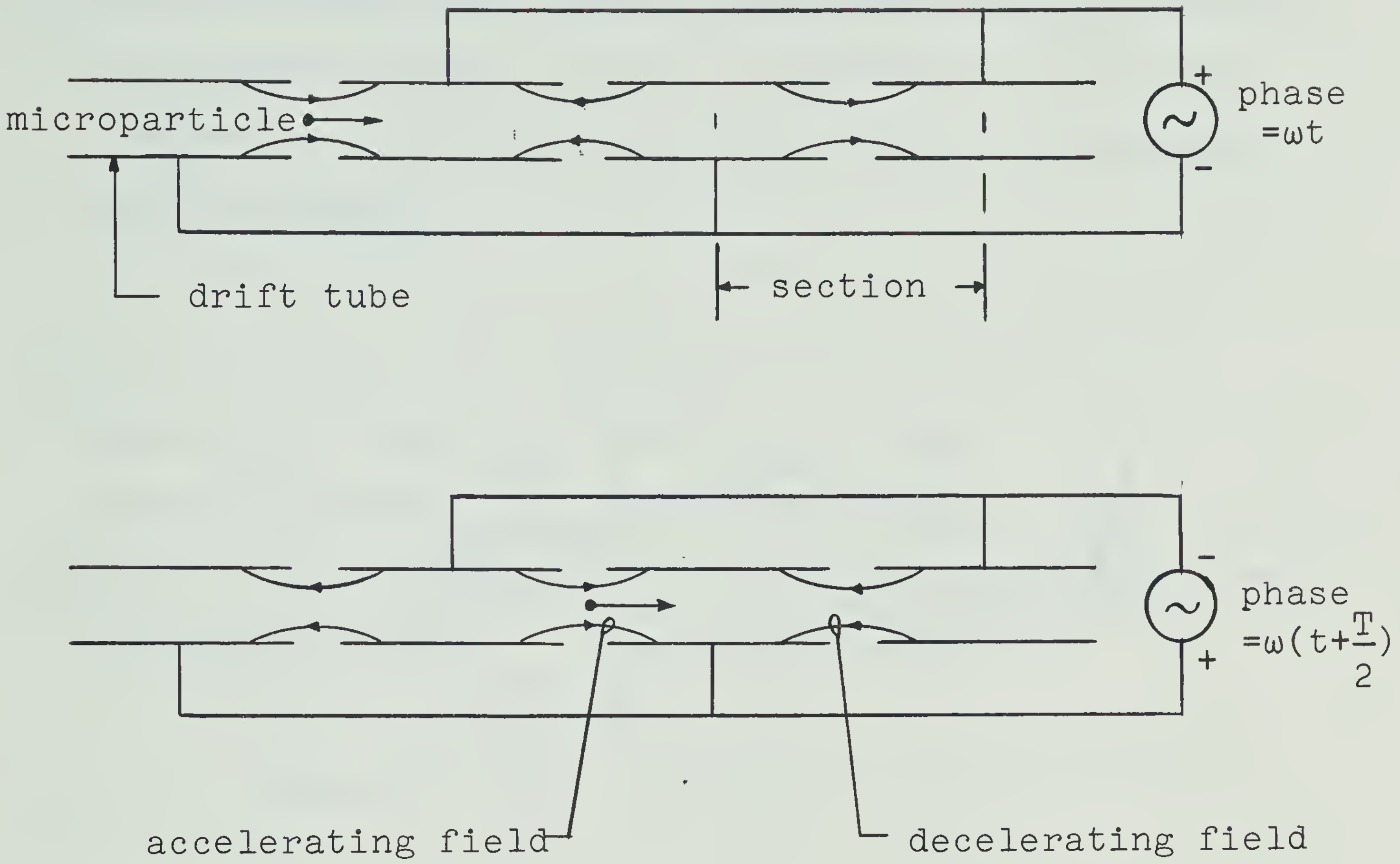

Fig. 2-1 Sloan-Lawrence Structure

In computing the motion of a particle in any given accelerating section i.e., the region between the centres of two successive drift tubes, the following simplifying assumptions are made:

1. It is assumed that the particle traverses the section at constant velocity. This is justified if the energy gained by the particle while traversing the section is small compared to the energy which the particle has when entering the section.

2. It is assumed that the particle traverses the section at constant radius. This is justified if the angle between the particle trajectory and the accelerator axis is small.

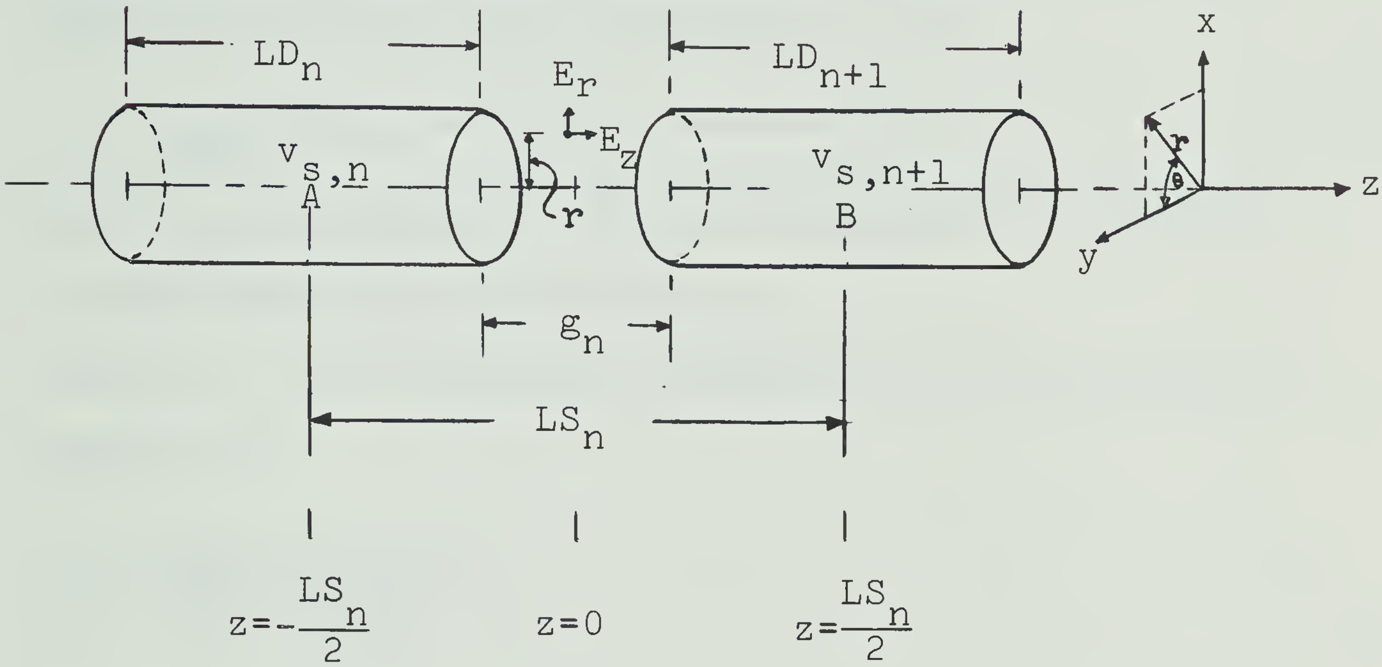

Note: g_n is the length of n^{th} gap; LD_n is the length of the n^{th} drift tube; LS_n is the length of n^{th} section; A and B are the mid points of the n^{th} and $(n+1)^{th}$ drift tubes respectively; $v_{s,n}$ is the constant velocity of the synchronous particle in a single section, i.e., between points A and B.

Fig. 2-2. A Single Section of the Sloan-Lawrence Structure

Fig. 2-2 shows the detailed dimensions of a single section of the Sloan-Lawrence structure. The synchronous particle takes a half-cycle to go from one gap centre to the next. As a consequence of this and the assumption No. 1 stated before, the particle will take a half-cycle

to traverse a single section. Thus the length of the n^{th} section is given by

$$LS_n = \left(v_{s,n}\right)\frac{T}{2} \text{ ---(2-3)}$$

In the following analysis those particles which are not synchronous, i.e., the nonsynchronous particles, are treated by writing their velocity v_n as

$$v_n = v_{s,n}/(1+k_n) \text{ -------------------------------------(2-4)}$$

where k_n is a parameter whose value, for any particle, changes from section to section.

Using 2-4, the independent variable ωt of 2-2 can be written as

$$\omega t = \left(\frac{2\Pi}{T}\right)\frac{Z(1+k_n)}{v_{s,n}}$$

which, by use of equation 2-3, becomes

$$\omega t = \left(\frac{\Pi Z}{LS_n}\right)(1+k_n) \text{ -------------------------------------(2-5)}$$

Because of the assumption 2 of the previous page the term containing $\dot{\theta}^2$ of 2-2 can be neglected.

Thus, substitution of the relation 2-5 in 2-2 yields

$$m\ddot{r} = qE_r(r,Z)\ \cos\left\{\frac{\Pi Z}{LS_n}\ (1+k_n)+\phi_n\right\}$$

Using the relation $\ddot{r} = v_n \frac{d\dot{r}}{dZ}$ in the foregoing equation one obtains

$$d\dot{r} = \frac{qE_r(r,Z)}{mv_n} \text{COS}\left\{\frac{\Pi Z}{LS_n}(1+k_n)+\phi_n\right\}dZ$$

Integration of the above equation from $-LS_n/2$ to $LS_n/2$ (refer to Fig. 2.2) yields

$$\Delta\dot{r}_n = \int_{-LS_n/2}^{LS_n/2} d\dot{r} = \frac{q}{mv_n}\int_{-LS_n/2}^{LS_n/2} E_r(r,Z)\ \text{COS}\left\{\frac{\Pi Z}{LS_n}(1+k_n)+\phi_n\right\}dZ \quad \text{------------------------(2-6)}$$

where $\Delta\dot{r}_n$ is the difference in radial velocity of the particle at the beginning and the end of the n^{th} section. From A1-6 of Appendix 1 it is seen that $E_r(r,Z)$ is an odd function of Z. Thus 2-6 becomes

$$\Delta\dot{r}_n = -\frac{q\ \text{SIN}(\phi_n)}{mv_n}\int_{-LS_n/2}^{LS_n/2} E_r(r,Z)\ \text{SIN}\left\{\frac{\Pi Z}{LS_n}(1+k_n)\right\}dZ$$

Assuming $k_n \ll 1$, the foregoing equation becomes

$$\Delta\dot{r}_n = -\frac{q\ \text{SIN}(\phi_n)}{mv_n}\left[\int_{-LS_n/2}^{LS_n/2} E_r(r,Z)\ \text{SIN}(\Pi Z/LS_n)\ dZ + k_n\int_{-LS_n/2}^{LS_n/2} \frac{\Pi Z}{LS_n} E_r(r,Z)\ \text{COS}(\Pi Z/LS_n)\ dZ\right] \quad \text{----------(2-7)}$$

[illegible]

From A2-3 and A2-5 of Appendix 2, the above equation becomes

$$\Delta\dot{r}_n = -\frac{V_m q \,\mathrm{SIN}(\phi_n)}{m v_n}\left[R - k_n LS_n \frac{dR}{dLS_n}\right] \text{------------------(2-8)}$$

where $R = T_{s,n}(0)\ I_1(\Pi r/LS_n)$

$$T_{s,n}(r) = \frac{\mathrm{SIN}\left(\frac{\Pi g_n}{2LS_n}\right)}{\frac{\Pi g_n}{2LS_n}} \cdot \frac{I_0(\Pi r/LS_n)}{I_0(\Pi a/LS_n)}$$

V_m = peak voltage at the gap.

$I_0(\Pi r/LS_n)$ and $I_1(\Pi r/LS_n)$ are the modified Bessel functions of first kind of zero and first order respectively.

If T_{nonsyn} is defined as the transit time factor of the nonsynchronous particle then equation 2-8 becomes

$$\Delta\dot{r}_n = -\frac{V_m q \,\mathrm{SIN}(\phi_n)}{m v_n} T_{nonsyn}$$

where

$$T_{nonsyn} = R - k_n LS_n \frac{dR}{dLS_n} \text{------------------------------(2-9)}$$

At this point one may note that for synchronous particle or almost synchronous particle ($k_n \simeq 0$), the equation 2-8 becomes

$$\Delta\dot{r}_n = -\frac{V_m q \ \mathrm{SIN}(\phi_n)}{m v_n}\left[T_{s,n}(0)\ I_1(\Pi r/LS_n)\right] \text{------------(2-10)}$$

Hence it is seen that for ϕ_s negative $\Delta\dot{r}_n$ is positive, i.e., the gap field is defocusing. On the otherhand, if ϕ_s is positive $\Delta\dot{r}_n$ is negative and the gap field is focusing.

2.1.2 Matrix Representation of Particle Motion

The entire effect of the accelerating gap on the radial motion of a particle is assumed to take place at the centre of the gap in the form of a δ-function. If the suffixes 1n and 2n denote quantities just to the left and to the right of the n^{th} gap centre, respectively, then the radial motion is described by

$$r_{2n} = r_{1n} \text{ ----------------------------------(2-11)}$$

and

$$\Delta\dot{r}_n = \dot{r}_{2n} - \dot{r}_{1n} = -\Delta_n r \text{ -----------------------(2-12)}$$

where, from 2-8

$$\Delta_n = \frac{V_m q \; SIN(\phi_n)}{mv_n} \left[\frac{R - k_n LS_n \dfrac{dR}{dLS_n}}{r} \right] \text{------------------(2-13)}$$

It is now recalled that for the purpose of computing the radial impulse of a particle it was assumed that the particle traversed the section at constant radius. This constant radius is taken to be that at the middle of the gap. Hence, it follows from 2-12

$$\Delta\dot{r}_n = -\Delta_n r_{1n} \text{-----------------------------------(2-14)}$$

From 2-11 and 2-14 the radial motion of the micro-particle at the gap centre can be written in the form of a transfer matrix as

$$\begin{pmatrix} r_{2n} \\ \dot{r}_{2n} \end{pmatrix} = \begin{pmatrix} 1 & 0 \\ -\Delta_n & 1 \end{pmatrix} \begin{pmatrix} r_{1n} \\ \dot{r}_{1n} \end{pmatrix} \text{----------------------------(2-15}$$

2.2 Axial Motion in the Accelerating Gap

2.2.1 General Equations and Assumptions

The assumptions in art.2.1.1 will also be used in this section. The equation of axial motion of the particle is derived from the Lorentz force equation 2-1 as

$$m\ddot{Z} = qE_Z(r,Z)\ \mathrm{COS}(\omega t + \phi) \quad \text{------------------------(2-16)}$$

From 2-5 and the foregoing equation one obtains the equation of axial motion of the particle in the n^{th} section as

$$m\ddot{Z} = qE_Z(r,Z)\ \mathrm{COS}\left\{\frac{\Pi Z}{LS_n}(1+k_n)+\phi_n\right\} \quad \text{-------------------(2-17)}$$

Use of the relation $\ddot{Z} = \frac{d\dot{Z}}{dZ} v_n$ in the above equation leads to

$$d\dot{Z} = \frac{q}{mv_n} E_Z(r,Z)\ \mathrm{COS}\left\{\frac{\Pi Z}{LS_n}(1+k_n)+\phi_n\right\} dZ$$

Integration of the foregoing equation from $-LS_n/2$ to $LS_n/2$ yields

$$\Delta\dot{Z}_n = \int_{-LS_n/2}^{LS_n/2} d\dot{Z} = \frac{q}{mv_n}\int_{-LS_n/2}^{LS_n/2} E_Z(r,Z)\ \mathrm{COS}\left\{\frac{\Pi Z}{LS_n}(1+k_n)+\phi_n\right\} dZ$$

$$\text{------------------------(2-18)}$$

where $\Delta\dot{Z}_n$ is the difference in axial velocity of the particle at the beginning and the end of the n^{th} section. Using A1-5 of the Appendix 1 the foregoing equation becomes

$$\Delta\dot{Z}_n = \left[\int_{-LS_n/2}^{LS_n/2} E_Z(r,Z) \cos\frac{\Pi Z}{LS_n}\, dZ - k_n \int_{-LS_n/2}^{LS_n/2} \left(\frac{\Pi Z}{LS_n}\right) E_Z(r,Z) \sin\left(\frac{\Pi Z}{LS_n}\right) dZ \right] \qquad \text{(2-19)}$$

Integration (refer to A2-7 and A2-8 of Appendix 2) of the above equation yields

$$\Delta\dot{Z}_n = \frac{V_m q \cos(\phi_n)}{m v_n} \left[T_{s,n}(r) + k_n LS_n \frac{dT_{s,n}(r)}{dLS_n} \right] \qquad \text{(2-20)}$$

In all numerical calculations the above change in velocity is assumed to take place at the middle of the gap in the form of a δ-function.

2.2.2 Energy Gain of a Microparticle

The energy gain ΔE_n of a microparticle in traversing the n^{th} section is

$$\Delta E_n = q\left[\int_{-LS_n/2}^{LS_n/2} E_Z(r,Z) \cos\left\{\frac{\Pi Z}{LS_n}(1+k_n)+\phi_n\right\} dZ \right.$$

$$\left. + \int_{r_1}^{r_2} E_r(r,Z) \cos\left\{\frac{\Pi Z}{LS_n}(1+k_n)+\phi_n\right\} dr \right] \qquad \text{(2-21)}$$

where r_1 and r_2 are the radial excursions of the particle at the beginning and the end of the n^{th} section respectively. If r' is the first order derivative of r w.r.t. Z then

$$dr = r' \, dZ$$

Using this relation in 2-21 and assuming r' is constant in the section, one obtains

$$\Delta E_n = q\left[\int_{-LS_n/2}^{LS_n/2} E_Z(r,Z)\ \mathrm{COS}\left\{\frac{\Pi Z}{LS_n}(1+k_n)+\phi_n\right\} dZ + r' \int_{-LS_n/2}^{LS_n/2} E_r(r,Z)\ \mathrm{COS}\left\{\frac{\Pi Z}{LS_n}(1+k_n)+\phi_n\right\} dZ\right]$$

Note that the radial force is computed as previously, i.e., by assuming that the particle traverses the gap at a fixed radius r. However, to compute the energy gain, the particle is permitted to undergo a radial displacement of $r' \, dZ$. Upon integration of the above two integrals (refer to 2-18 and 2-20 for the first integral and 2-6, 2-8 for the second integral) the above equation becomes

$$\Delta E_n = V_m q\left[\cos(\phi_n)\left\{T_{s,n}(r)+k_n LS_n\frac{dT_{s,n}(r)}{dLS_n}\right\} - r' \sin(\phi_n)\left\{R-k_n LS_n\frac{dR}{dLS_n}\right\}\right] \quad \text{-----------------(2-22)}$$

2.2.3 Incompatibility between Radial and Axial Stability

The condition of radial stability, i.e., the radial focusing of an accelerating particle has already been discussed in section 2.1.1. The condition of axial stability, i.e., the presence of net axial restoring force toward the position of the synchronous particle is derived as follows:

The Z coordinate of the synchronous particle may be written as

$$Z = Z_s + \delta$$

where δ is the Z coordinate of the nonsynchronous particle referred to that of the synchronous particle.

Equation 2-17 then becomes

$$m(\ddot{Z}_s+\ddot{\delta}) = qE_Z(r,Z_s+\delta)\ \cos\left\{\frac{\Pi(Z_s+\delta)}{LS_n}(1+k_n)+\phi_n\right\}$$

Expanding $E_Z(r,Z_s+\delta)$ in Taylor's series about $E_Z(r,Z_s)$ and

neglecting the higher order terms of δ the above equation becomes

$$m(\ddot{Z}_s+\ddot{\delta}) = q\left[E_Z(r,Z_s)+\delta\frac{\partial E_Z(r,Z_s)}{\partial Z_s}\right]\cos\left\{\frac{\Pi(Z_s+\delta)}{LS_n}+\phi_n\right\}$$

$$= qE_Z(r,Z_s)\cos\left\{\frac{\Pi(Z_s+\delta)}{LS_n}+\phi_n\right\}$$

$$+\ q\delta\frac{\partial E_Z(r,Z_s)}{\partial Z_s}\cos\left\{\frac{\Pi(Z_s+\delta)}{LS_n}+\phi_n\right\}$$

If one assumes $\Delta Z<<Z_s$, $k_n<<1$, and $\phi_n\simeq\phi_s$, then the foregoing equation can be written as

$$m\ddot{\delta} = q\delta\frac{\partial E_Z(r,Z_s)}{\partial Z_s}\cos\left\{\frac{\Pi Z_s}{LS_n}+\phi_s\right\}$$

Use of the relation $\ddot{\delta} = \frac{d\dot{\delta}}{dZ_s}v_{s,n}$ in the above equation yields

$$d\dot{\delta} = \frac{q\delta}{mv_{s,n}}\ \frac{\partial E_Z(r,Z_s)}{\partial Z_s}\cos\left\{\frac{\Pi Z_s}{LS_n}+\phi_s\right\}dZ_s$$

Integrating the above equation from $-LS_n/2$ to $LS_n/2$, one obtains

$$\Delta\dot{\delta}_n = \int_{-LS_n/2}^{LS_n/2} d\dot{\delta} = \frac{q}{mv_{s,n}}\int_{-LS_n/2}^{LS_n/2}\delta\frac{\partial E_Z(r,Z_s)}{\partial Z_s}\cos\left\{\frac{\Pi Z_s}{LS_n}+\phi_s\right\}dZ_s$$

where $\Delta\dot{\delta}_n$ is the difference in relative axial velocity of the particle with respect to synchronous particle at the beginning and the end of the n^{th} section. Assuming that the particle crosses the section at constant δ and using the result

$$\int_{-LS_n/2}^{LS_n/2} \frac{\partial E_Z(r,Z_s)}{\partial Z_s} \cos\left(\frac{\Pi Z_s}{LS_n}\right) dZ_s = 0$$

the foregoing equation becomes

$$\Delta\dot{\delta}_n = -\frac{q\delta \sin(\phi_s)}{mv_{s,n}} \int_{-LS_n/2}^{LS_n/2} \frac{\partial E_Z(r,Z_s)}{\partial Z_s} \sin\left(\frac{\Pi Z_s}{LS_n}\right) dZ_s$$

Upon integration by parts and assuming E_Z is zero at $\pm LS_n/2$, the above equation can be written as

$$\Delta\dot{\delta}_n = \left(\frac{q\delta \sin(\phi_s)}{mv_{s,n}}\right)\left(\frac{\Pi}{LS_n}\right) \int_{-LS_n/2}^{LS_n/2} E_Z(r,Z_s) \cos\frac{\Pi Z_s}{LS_n}\, dZ$$

Use of A2-7 of Appendix 2 in the above equation yields

$$\Delta\dot{\delta}_n = \frac{\Pi q\delta \sin(\phi_s)}{LS_n \cdot mv_{s,n}} \left\{T_{s,n}(r)\ V_m\right\} \text{--------------------(2-23}$$

From the foregoing equation it is seen that for ϕ_s positive $\Delta\dot{\delta}_n$ is positive, i.e., the gap field forces are defocusing and the particle under consideration moves away from the synchronous particle. On the other hand for ϕ_s negative $\Delta\dot{\delta}_n$ is negative, and the above effect is reversed. From the foregoing result and by recalling that the radial focusing occurs for positive ϕ_s it is concluded that radial stability and axial stability cannot be achieved simultaneously for the type of accelerating gap considered. This phenomenon of incompatibility is known as Macmillan's theorem. As a compromise between those two conflicting stability conditions the synchronous phase ϕ_s is always chosen close to zero. There are no suitable methods which can eliminate the axial instability of particles if ϕ_s is positive. However, there are various methods which can be used to eliminate the radial defocusing effect of the gap if ϕ_s is negative. For this reason ϕ_s is always chosen negative. In that case small radial defocusing of the gap field can be compensated for by an auxiliary focusing system. In this study the auxiliary system consists of electrostatic quadrupoles which are placed co-axially within the drift tubes.

2.3 Motion of a Particle in a Drift Tube with an Electrostatic Quadrupole

An electrostatic quadrupole consists of 4 rectangular hyperbolic electrodes which are alternately positive and negative, and are symmetrically placed about the axis of the accelerator as shown in Fig. 2-3.

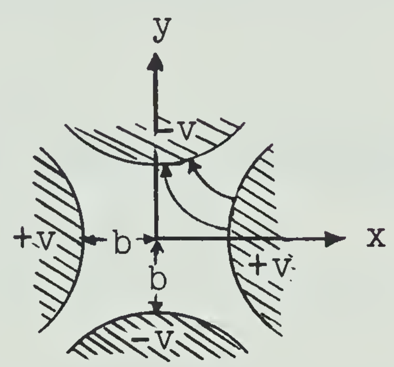

Fig. 2-3 Sectional View of the Field Lines Between Quadrupoles

A solution to Laplace's equation in the region between the hyperbolic surfaces, and which can be made to satisfy the appropriate boundary conditions is given by

$$\Psi = \frac{1}{2}k\ (x^2-y^2) \qquad (2\text{-}24)$$

Since $\quad \Psi = +V \quad$ at $\quad \frac{x^2}{b^2} - \frac{y^2}{b^2} = 1$

and $\quad \Psi = -V \quad$ at $\quad \frac{x^2}{b^2} - \frac{y^2}{b^2} = -1$

one obtains that

$$k = \frac{2V}{b^2} \tag{2-25}$$

where 2V is the voltage between the quadrupoles.

Hence, from $E = -\nabla\Psi$ it follows that

$$E_x = -\frac{2V}{b^2}x \tag{2-26}$$

$$E_y = \frac{2V}{b^2}y \tag{2-27}$$

Consequently, the equations of motion for a particle of charge q are

$$\left.\begin{aligned} \ddot{x} &= -Q^2 x \\ \ddot{y} &= Q^2 y \end{aligned}\right\} \tag{2-28}$$

where $\quad Q^2 = \frac{2V}{b^2}\ \frac{q}{m} \qquad (2\text{-}29)$

Evidently, for a positively charged particle the motion in the x-direction is focused, while the motion in the y-direction is defocused.

The solutions to 2-28 are

$$x = a_1 \text{ COS}(Qt) + a_2 \text{ SIN}(Qt) \text{ ----------------(2-30)}$$

$$y = a_3 \text{ COSH}(Qt) + a_4 \text{ SINH}(Qt) \text{ ---------------(2-31)}$$

and $$\dot{x} = -a_1 Q \text{ SIN}(Qt) + a_2 Q \text{ COS}(Qt) \text{ --------------(2-32)}$$

$$\dot{y} = a_3 Q \text{ SINH}(Qt) + a_4 Q \text{ COSH}(Qt) \text{ -------------(2-33)}$$

where a_1, a_2, a_3 and a_4 are constants.

With the assumption that the velocity v_n of the particle remains constant while passing the (n^{th}) quadrupole, one may write the time spent in the (n^{th}) quadrupole as

$$T_n = \frac{LQ_n}{v_n}$$

where LQ_n is the length of the n^{th} quadrupole.

If $t = 0$ when the particle enters the quadrupole, then at $t = T_n/2$ the particle will have reached the transverse plane at the middle of the quadrupole.

Denoting the quantities at the entrance and the midplane of the quadrupole by subscripts 0 and 1 respectively, one obtains from 2-30, 2-31, 2-32, and 2-33

$$x_0 = a_1, \quad \dot{x}_0 = a_2 Q$$

$$y_0 = a_3, \quad \dot{y}_0 = a_4 Q$$

$$x_1 = a_1 \cos\left(\frac{QT_n}{2}\right) + a_2 \sin\left(\frac{QT_n}{2}\right)$$

$$\dot{x}_1 = -a_1 Q \sin\left(\frac{QT_n}{2}\right) + a_2 Q \cos\left(\frac{QT_n}{2}\right)$$

$$y_1 = a_3 \cosh\left(\frac{QT_n}{2}\right) + a_4 \sinh\left(\frac{QT_n}{2}\right)$$

$$\dot{y}_1 = a_3 Q \sinh\left(\frac{QT_n}{2}\right) + a_4 Q \cosh\left(\frac{QT_n}{2}\right)$$

From the above relations one finally obtains the motion of the particle in the first half-length of the quadrupole, in matrix form as follows:

in the focusing plane

$$\begin{pmatrix} x_1 \\ \dot{x}_1 \end{pmatrix}_n = \begin{pmatrix} \cos\left(\frac{QT_n}{2}\right) & \frac{1}{Q} \sin\left(\frac{QT_n}{2}\right) \\ -Q \sin\left(\frac{QT_n}{2}\right) & \cos\left(\frac{QT_n}{2}\right) \end{pmatrix} \begin{pmatrix} x_0 \\ \dot{x}_0 \end{pmatrix}_n = T_F \begin{pmatrix} x_0 \\ \dot{x}_0 \end{pmatrix}_n$$

------------------------(2-34)

in the defocusing plane

$$\begin{pmatrix} y_1 \\ \\ \dot{y}_1 \end{pmatrix}_n = \begin{pmatrix} \text{COSH } \frac{QT_n}{2} & \frac{1}{Q} \text{ SINH } \frac{QT_n}{2} \\ \\ Q \text{ SINH } \frac{QT_n}{2} & \text{COSH } \frac{QT_n}{2} \end{pmatrix} \begin{pmatrix} y_0 \\ \\ \dot{y}_0 \end{pmatrix}_n = T_D \begin{pmatrix} y_0 \\ \\ \dot{y}_0 \end{pmatrix}_n$$

-------------------------(2-35)

where T_F and T_D are called the transfer matrices in the focusing and the defocusing planes respectively.

It can readily be shown that if T_F' and T_D' are the transfer matrices in the focusing and the defocusing planes, respectively, of the second half-length of the quadrupoles then

$$T_F' = T_F \quad \text{--------------------------------(2-36)}$$

$$T_D' = T_D \quad \text{--------------------------------(2-37)}$$

2.4 Transfer Matrix for the Radial Motion of a Particle for One Repeat Section

In this study the quadrupoles are arranged so that the axes x-y are rotated through 90° in successive drift tubes. Thus the particle traveling in the focusing plane

(y=0 plane) in one drift tube will travel in the defocusing plane (x=0 plane) in the next (refer to Fig. 2-4) so that the focusing and the defocusing action in a plane is

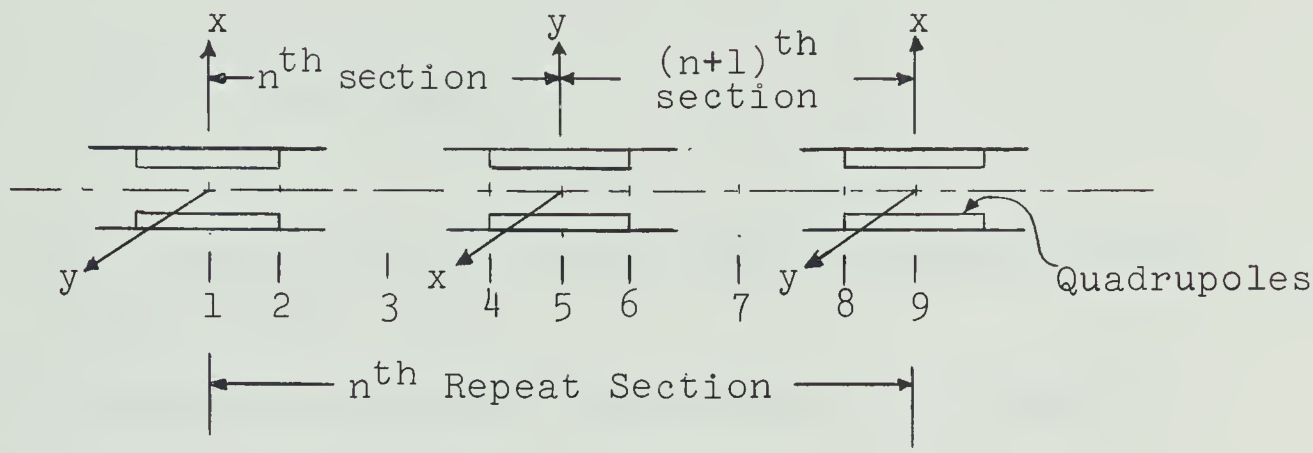

Fig. 2-4 One Repeat Length of the Quadrupole Focused Linear Accelerator

repeated after alternate drift tubes. The length between alternate drift tubes is known as one repeat length. The transfer matrices T^{12}, T^{45}, T^{56}, T^{89}, T^{3}, and T^{7} for the regions 1-2, 4-5, 5-6, 8-9 and the gap centres 3 and 7 respectively have already been derived and are shown in equations 2-34, 2-35 and 2-15. To formulate the transfer matrix of the complete repeat section shown in Fig. 2-4 one has yet to find out the transfer matrices T^{23}, T^{34}, T^{67} and T^{78} of the drift regions 2-3, 3-4, 6-7 and 7-8 respectively. Since the particle traverses these drift

regions at constant velocities one can write the equation of radial motion for a particle in the region 2-3 as

$$\dot{r}_3 = \dot{r}_2$$

$$r_3 = r_2 + \dot{r}_2 t_{23}$$

where $t_{23} = L_{23}/v_n$ and L_{23} is the length between the sections 2 and 3 in Fig. 2-4.

The foregoing equations are written in the matrix form as

$$\begin{pmatrix} r_3 \\ \dot{r}_3 \end{pmatrix} = \begin{pmatrix} 1 & t_{23} \\ 0 & 1 \end{pmatrix} \begin{pmatrix} r_2 \\ \dot{r}_2 \end{pmatrix} \quad \text{------------------------------}(2\text{-}38)$$

Thus the transfer matrix T_{23} for the radial motion of the particle between the sections 2 and 3 is

$$T^{23} = \begin{pmatrix} 1 & t_{23} \\ 0 & 1 \end{pmatrix} \quad \text{------------------------------------}(2\text{-}39)$$

In a similar way one can find the transfer matrices T^{34}, T^{67} and T^{78}. It is evident that the above transfer matrix 2-39 for r and $\dot{r}$ is also valid for x and $\dot{x}$, and y and $\dot{y}$. Hence, the equation describing the motion parallel

to the plane of the paper in Fig. 2-4, i.e., in the vertical plane and between the sections 1 and 5 can be written as

$$\begin{pmatrix} y_5 \\ \\ \dot{y}_5 \end{pmatrix}_N = T^{45}\, T^{34}\, T^{3}\, T^{23}\, T^{12} \begin{pmatrix} x_1 \\ \\ \dot{x}_1 \end{pmatrix}_N = T_{\alpha N} \begin{pmatrix} x_1 \\ \\ \dot{x}_1 \end{pmatrix}_N \quad \text{------(2-40)}$$

where

$$T_{\alpha N} = T^{45}\, T^{34}\, T^{3}\, T^{23}\, T^{12} \quad \text{------(2-41)}$$

Similarly the matrix equation between the sections 5 and 9 is

$$\begin{pmatrix} x_9 \\ \\ \dot{x}_9 \end{pmatrix}_N = T^{89}\, T^{78}\, T^{7}\, T^{67}\, T^{56} \begin{pmatrix} y_5 \\ \\ \dot{y}_5 \end{pmatrix}_N = T_{\beta N} \begin{pmatrix} y_5 \\ \\ \dot{y}_5 \end{pmatrix}_N \quad \text{------(2-42)}$$

where

$$T_{\beta N} = T^{89}\, T^{78}\, T^{7}\, T^{67}\, T^{56} \quad \text{------(2-43)}$$

From 2-40 and 2-42 the equation of motion between the sections 1 and 9 in the vertical plane is

$$\begin{pmatrix} x_9 \\ \dot{x}_9 \end{pmatrix}_N = T_{\beta N}\, T_{\alpha N} \begin{pmatrix} x_1 \\ \dot{x}_1 \end{pmatrix}_N = T_N \begin{pmatrix} x_1 \\ \dot{x}_1 \end{pmatrix}_N \text{ ------------------(2-44)}$$

where

$$T_N = T_{\beta N}\, T_{\alpha N} \text{ ------------------------------------(2-45)}$$

T_N is the transfer matrix for the N^{th} repeat section in the vertical plane.

It is evident from the foregoing analysis that the particle motion perpendicular to the plane of the paper in Fig. 2-4, i.e., in the horizontal plane and between the sections 1 and 9 is given by

$$\begin{pmatrix} y_9 \\ \dot{y}_9 \end{pmatrix}_N = T'_N \begin{pmatrix} y_1 \\ \dot{y}_1 \end{pmatrix}_N \text{ ---------------------------------(2-46)}$$

where $T'_N = T_{\alpha N} T_{\beta N}$ ---------------------------------(2-47)

T'_N is the transfer matrix for the N^{th} repeat section in the horizontal plane.

CHAPTER 3

SOME PROPERTIES OF PARTICLE MOTION IN THE TRANSVERSE PLANE IN A LINEAR ACCELERATOR WITH ELECTROSTATIC QUADRUPOLES

3.1 General Equations

T_N and T_N', the transfer matrices for the transverse motion, change from one repeat section to the next. So it is very complicated to study the transverse behaviour of the beam analytically. In the next chapter a numerical study of the beam properties will be made, taking into proper account the variation of T_N and T_N' with N. In the present chapter the beam is studied analytically with the simplifying assumption that T_N and T_N' are the same for all N. This approach does not yield an exact answer, however it provides a great amount of physical insight into the transverse behaviour of the particle beam. In particular then the assumptions made in this chapter are the following:

1. The particle traverses the accelerator at constant velocity and phase.
2. The repeat sections are identical in all respects and symmetric about the middle plane transverse to the axis of the accelerator.

By the foregoing assumptions one can write T_N and T_N' as

$$T_1 = T_2 = \ldots\ldots = T_N = T = \begin{pmatrix} T_{11} & T_{12} \\ T_{21} & T_{22} \end{pmatrix} \text{-------------}(3\text{-}1)$$

$$T_1' = T_2' = \ldots\ldots = T_N' = T' = \begin{pmatrix} T_{11}' & T_{12}' \\ T_{21}' & T_{22}' \end{pmatrix} \text{-------}(3\text{-}2)$$

where T_{11}, T_{12}, T_{21} and T_{22} are the elements of the transfer matrix T of one repeat section between focusing and focusing and T_{11}', T_{12}' , T_{21}' and T_{22}' are the elements of the transfer matrix T' of one repeat section between defocusing and defocusing.

Now if the vertical planes in the first drift tube are assumed to be focusing then the vertical planes in each alternate drift tube will also be focusing. Thus one can write

$$\begin{pmatrix} x \\ \dot{x} \end{pmatrix}_p = T_p \; T_{p-1} \; \ldots \; T_1 \begin{pmatrix} x \\ \dot{x} \end{pmatrix}_0$$

where $\begin{pmatrix} x \\ \dot{x} \end{pmatrix}_0$ and $\begin{pmatrix} x \\ \dot{x} \end{pmatrix}_p$ are the coordinate vectors in the

vertical planes and at the beginning of the first and the end of the p^{th} repeat section respectively.

By use of 3-1 the foregoing equation becomes

$$\begin{pmatrix} x \\ \dot{x} \end{pmatrix}_p = T^p \begin{pmatrix} x \\ \dot{x} \end{pmatrix}_0 \quad \text{-------------------------------------(3-3)}$$

Similarly in the horizontal and the defocusing planes

$$\begin{pmatrix} y \\ \dot{y} \end{pmatrix}_p = T'^p \begin{pmatrix} y \\ \dot{y} \end{pmatrix}_0 \quad \text{------------------------------------(3-4)}$$

where $\begin{pmatrix} y \\ \dot{y} \end{pmatrix}_0$ and $\begin{pmatrix} y \\ \dot{y} \end{pmatrix}_p$ are the coordinate vectors in the horizontal planes and at the beginning of the first and the end of the p^{th} repeat section respectively.

3.2 Radial Stability

By definition radial stability means that all the elements of the transfer matrices T^p and T'^p remain bounded as p increases indefinitely. This condition is necessary and sufficient.

The required condition for stability for T^p is arrived at in the following way:

If λ is one of the eigenvalues of the matrix T, and if use is made of the relation[13] $\det T = 1$, then the characteristic equation of T is

$$\lambda^2-\lambda(T_{11}+T_{22}) + 1 = 0$$

or,

$$\lambda_i = \frac{(T_{11}+T_{22})\pm\sqrt{(T_{11}+T_{22})^2-4}}{2} \qquad \text{(3-5)}$$

where i = 1,2

To diagonalize T it is written as follows

$$T = ADA^{-1} \qquad \text{(3-6)}$$

where A is the transform matrix and D is the diagonal matrix with λ_i as the diagonal elements i.e., $D = \begin{pmatrix} \lambda_1 & 0 \\ 0 & \lambda_2 \end{pmatrix}$

Hence

$$D^p = \begin{pmatrix} \lambda_1^p & 0 \\ 0 & \lambda_2^p \end{pmatrix} \qquad \text{(3-7)}$$

where p is an integer.

Thus from 3-6 and 3-7

$$T^p = A(\lambda_i^p)\ A^{-1} \text{ -- } (3\text{-}8)$$

Thus, λ_i^p is the only p dependent term in the matrix T^p. This means that the elements of the transfer matrix T^p will be finite for any p if and only if

$$|\lambda_i| \le 1 \text{ -- } (3\text{-}9)$$

Thus from 3-5 and 3-9 one obtains

$$\left|\left(\frac{T_{11}+T_{22}}{2}\right) \pm \sqrt{\left(\frac{T_{11}+T_{22}}{2}\right)^2-1}\right| \le 1 \text{ -------------------- } (3\text{-}10)$$

It follows that

$$\left|T_{11}+T_{22}\right| \le 2 \text{ --------------------------------------- } (3\text{-}11)$$

implies stability,

$$\left|T_{11}+T_{22}\right| > 2 \text{ --------------------------------------- } (3\text{-}12)$$

implies instability.

Similarly

$$\left| T'_{11} + T'_{22} \right| \leq 2 \text{ ---------------------------------(3-13)}$$

assures stability and

$$\left| T'_{11} + T'_{22} \right| > 2 \text{ ---------------------------------(3-14)}$$

means instability.

3.3 Equation of Transverse Motion for a Stable Particle

Because of the assumptions of periodicity in section 3.1, $T_{\alpha N}$ and $T_{\beta N}$ of equations 2-41 and 2-43 respectively can be written as

$$T_{\alpha 1} = T_{\alpha 2} = \ldots\ldots = T_{\alpha N} = T_{\alpha} = \begin{pmatrix} \alpha_{11} & \alpha_{12} \\ \alpha_{21} & \alpha_{22} \end{pmatrix} \text{---------(3-15)}$$

and

$$T_{\beta 1} = T_{\beta 2} = \ldots\ldots = T_{\beta N} = T_{\beta} = \begin{pmatrix} \beta_{11} & \beta_{12} \\ \beta_{21} & \beta_{22} \end{pmatrix} \text{---------(3-16)}$$

where α_{11}, α_{12}, α_{21} and α_{22} are the elements of the transfer matrix T_α of one half repeat section between focusing to defocusing. β_{11}, β_{12}, β_{21} and β_{22} are the elements of the transfer matrix T_β of one half repeat section between defocusing to focusing.

It can be shown that since the repeat section is symmetric about the middle plane transverse to the accelerator axis the following identity[13] holds

$$\begin{pmatrix} \alpha_{11} & \alpha_{12} \\ \alpha_{21} & \alpha_{22} \end{pmatrix} = \begin{pmatrix} \beta_{22} & \beta_{12} \\ \beta_{21} & \beta_{11} \end{pmatrix} \text{------------------------------(3-17)}$$

Thus from 3-1, 3-2, 3-15, 3-16, 3-17, 2-45 and 2-47 one obtains

$$\begin{pmatrix} T_{11} & T_{12} \\ T_{21} & T_{22} \end{pmatrix} = \begin{pmatrix} \alpha_{11}\alpha_{22}+\alpha_{12}\alpha_{21} & 2\alpha_{22}\alpha_{12} \\ 2\alpha_{11}\alpha_{21} & \alpha_{11}\alpha_{22}+\alpha_{12}\alpha_{21} \end{pmatrix} \text{-----(3-18)}$$

and

$$\begin{pmatrix} T'_{11} & T'_{12} \\ T'_{21} & T'_{22} \end{pmatrix} = \begin{pmatrix} \alpha_{11}\alpha_{22}+\alpha_{12}\alpha_{21} & 2\alpha_{11}\alpha_{12} \\ 2\alpha_{22}\alpha_{21} & \alpha_{11}\alpha_{22}+\alpha_{12}\alpha_{21} \end{pmatrix} \text{-----(3-19)}$$

From 3-18 and 3-19 it follows that

$$T_{11} = T_{22} = T'_{11} = T'_{22} = \alpha_{11}\alpha_{22}+\alpha_{12}\alpha_{21} \text{ ------------ } (3\text{-}20)$$

$$\frac{T_{12}}{T_{21}} = \frac{\alpha_{22}\alpha_{12}}{\alpha_{11}\alpha_{21}} \text{ ------------ } (3\text{-}21)$$

$$\frac{T'_{12}}{T'_{21}} = \frac{\alpha_{11}\alpha_{12}}{\alpha_{22}\alpha_{21}} \text{ ------------ } (3\text{-}22)$$

From the stability conditions 3-11, 3-13 and the equation 3-20 one can write for a stable particle

$$\frac{T_{11}+T_{22}}{2} = \frac{T'_{11}+T'_{22}}{2} = \mathrm{COS}(\mu) \text{ ------------ } (3\text{-}23)$$

where μ is real.

From 3-20 and 3-23 it follows that

$$T_{11} = T_{22} = T'_{11} = T'_{22} = \mathrm{COS}(\mu) \text{ ------------ } (3\text{-}24)$$

From 3-24 and the fact that det T = det T′ = 1[13] one can write

$$T_{12}T_{21} = -\ \mathrm{SIN}^2(\mu) \text{ ------------ } (3\text{-}25)$$

$$T'_{12}T'_{21} = -\mathrm{SIN}^2(\mu) \text{ ------------------------------ } (3\text{-}26)$$

To find T_{12} and T_{21}, 3-21 is written as

$$\frac{T_{12}}{T_{21}} = \frac{\alpha_{22}\alpha_{12}}{\alpha_{11}\alpha_{21}} = -\beta^2 \text{ ------------------------------ } (3\text{-}27)$$

From 3-25 and 3-27 one obtains

$$T_{12} = \beta\ \mathrm{SIN}(\mu) \text{ ------------------------------ } (3\text{-}28)$$

$$T_{21} = -\frac{\mathrm{SIN}(\mu)}{\beta} \text{ ------------------------------ } (3\text{-}29)$$

From 3-22 and 3-27 it follows that

$$\frac{T'_{12}}{T'_{21}} = -\beta^2 \bigg/ \left(\frac{\alpha_{22}}{\alpha_{11}}\right)^2 \text{ ------------------------------ } (3\text{-}30)$$

If one takes

$$\frac{\alpha_{22}}{\alpha_{11}} = \theta^2 \text{ ------------------------------ } (3\text{-}31)$$

equation 3-30 becomes

$$\frac{T'_{12}}{T'_{21}} = -\frac{\beta^2}{\theta^4} \text{ ------------------------------ } (3\text{-}32)$$

Then substitution of 3-32 in 3-26 yields

$$T'_{12} = \frac{\beta}{\theta^2} \text{SIN}(\mu) \text{ ----------------------------------(3-33)}$$

$$T'_{21} = -\frac{\theta^2}{\beta} \text{SIN}(\mu) \text{ ---------------------------------(3-34)}$$

Thus from 3-24, 3-28, 3-29, 3-33 and 3-34 the transfer matrices T and T' can be written as

$$T = \begin{pmatrix} \text{COS}(\mu) & \beta \text{ SIN}(\mu) \\ -\frac{1}{\beta} \text{SIN}(\mu) & \text{COS}(\mu) \end{pmatrix} \text{------------------------(3-35)}$$

$$T' = \begin{pmatrix} \text{COS}(\mu) & \frac{\beta}{\theta^2} \text{SIN}(\mu) \\ -\frac{\theta^2}{\beta} \text{SIN}(\mu) & \text{COS}(\mu) \end{pmatrix} \text{----------------------(3-36)}$$

Thus, from 3-3 and 3-4 and the foregoing equations the equations of transverse motion of the stable particle are

$$\begin{pmatrix} x \\ \dot{x} \end{pmatrix}_p = T^p \begin{pmatrix} x \\ \dot{x} \end{pmatrix}_0 = \begin{pmatrix} \text{COS}(p\mu) & \beta \text{ SIN}(p\mu) \\ -\frac{1}{\beta} \text{SIN}(p\mu) & \text{COS}(p\mu) \end{pmatrix} \begin{pmatrix} x \\ \dot{x} \end{pmatrix}_0 \text{ ----(3-37)}$$

$$\begin{pmatrix} y \\ \\ \dot{y} \end{pmatrix}_p = T^p \begin{pmatrix} y \\ \\ \dot{y} \end{pmatrix}_p = \begin{pmatrix} \cos(p\mu) & \frac{\beta}{\theta^2} \sin(p\mu) \\ \\ -\frac{\theta^2}{\beta} \sin(p\mu) & \cos(p\mu) \end{pmatrix} \begin{pmatrix} y \\ \\ \dot{y} \end{pmatrix}_0 \quad \text{---(3-38)}$$

where $\begin{pmatrix} x \\ \dot{x} \end{pmatrix}_0$ and $\begin{pmatrix} y \\ \dot{y} \end{pmatrix}_0$ are the coordinate vectors of the injected particle in the vertical and the horizontal planes respectively and $\begin{pmatrix} x \\ \dot{x} \end{pmatrix}_p$ and $\begin{pmatrix} y \\ \dot{y} \end{pmatrix}_p$ are the coordinate vectors of the particles at the end of the p^{th} repeat section and in the vertical and the horizontal planes respectively.

Similarly the equations of transverse motion at the middle of any repeat section are

$$\begin{pmatrix} y \\ \\ \dot{y} \end{pmatrix}_{p+\frac{1}{2}} = T_\alpha T^p \begin{pmatrix} x \\ \\ \dot{x} \end{pmatrix}_0$$

$$= \begin{pmatrix} \alpha_{11} \cos(p\mu) - \frac{\alpha_{12}}{\beta} \sin(p\mu) & \alpha_{11}\beta \sin(p\mu) + \alpha_{12} \cos(p\mu) \\ \\ \alpha_{21} \cos(p\mu) - \frac{\alpha_{22}}{\beta} \sin(p\mu) & \alpha_{21}\beta \sin(p\mu) + \alpha_{22} \cos(p\mu) \end{pmatrix} \begin{pmatrix} x \\ \\ \dot{x} \end{pmatrix}_0$$

$$\text{-----------------------(3-39)}$$

and

$$\begin{pmatrix} x \\ \\ \dot{x} \end{pmatrix}_{p+\frac{1}{2}} = T_\beta T'^p \begin{pmatrix} y \\ \\ \dot{y} \end{pmatrix}_0$$

$$= \begin{pmatrix} \beta_{11} \cos(p\mu) - \frac{\theta^2 \beta_{12}}{\beta} \sin(p\mu) & \frac{\beta_{11}\beta}{\theta^2} \sin(p\mu) + \beta_{12} \cos(p\mu) \\ \\ \beta_{21} \cos(p\mu) - \frac{\theta^2 \beta_{22}}{\beta} \sin(p\mu) & \frac{\beta_{21}\beta}{\theta^2} \sin(p\mu) + \beta_{22} \cos(p\mu) \end{pmatrix} \begin{pmatrix} y \\ \\ \dot{y} \end{pmatrix}_0$$

$$\text{-----------------------(3-40)}$$

where $\begin{pmatrix} y \\ \dot{y} \end{pmatrix}_{p+\frac{1}{2}}$ and $\begin{pmatrix} x \\ \dot{x} \end{pmatrix}_{p+\frac{1}{2}}$ are the coordinate vectors at the middle of the $(p+1)^{th}$ repeat section and in the vertical and horizontal planes respectively.

3.4 Acceptance of Particles in the Transverse Plane

In order that the particles are transmitted through the length of the accelerator, it is necessary that the finite excursions of the particles, as described by equations 3-37 and 3-38, do not exceed the distance "b" from the axis of the accelerator to the tips of the quadrupole electrodes. The object of this section is to compute the initial conditions of the particles so that the above boundary condition is not violated.

By elimination of $p\mu$ from equations 3-37 and 3-38 of the previous section one obtains

$$x_p^2 + \beta^2 \dot{x}_p^2 = x_0^2 + \beta^2 \dot{x}_0^2 \quad \text{--------------------------(3-41)}$$

$$y_p^2 + \frac{\beta}{\theta^4} \dot{y}_p^2 = y_0^2 + \frac{\beta}{\theta^4} \dot{y}_0^2 \quad \text{------------------------(3-42)}$$

Similarly by eliminating $p\mu$ from equations 3-39 and 3-40 one obtains

$$y_{p+\frac{1}{2}}^2\ (\alpha_{22}^2+\beta^2\alpha_{21}^2)+(\alpha_{12}^2+\beta^2\alpha_{11}^2)\dot{y}_{p+\frac{1}{2}}^2\ -2(\alpha_{12}\alpha_{22}+\beta^2\alpha_{11}\alpha_{21})y_{p+\frac{1}{2}}\dot{y}_{p+\frac{1}{2}}$$

$$= x_0^2\ +\beta^2\ \dot{x}_0^2 \quad \text{------------------------}(3\text{-}43)$$

and

$$x_{p+\frac{1}{2}}^2\ (\alpha_{11}^2+\frac{\beta^2}{\theta^4}\alpha_{21}^2)+\dot{x}_{p+\frac{1}{2}}\ (\alpha_{12}^2+\frac{\beta^2}{\theta^4}\alpha_{22}^2)-2x_{p+\frac{1}{2}}\dot{x}_{p+\frac{1}{2}}(\alpha_{11}\alpha_{12}+\frac{\beta^2}{\theta^4}\alpha_{21}\alpha_{22})$$

$$= y_0^2\ +\ \frac{\beta^2}{\theta^4}\dot{y}_0^2 \quad \text{----------------------}(3\text{-}44)$$

The equations 3-41 and 3-42 represent the equations of ellipses whose major and minor axes are coinciding with the coordinate axes, and the equations 3-43 and 3-44 represent the general equations of ellipses whose axes rotated clockwise through the angles ϕ_x and ϕ_y respectively where

$$\phi_x\ = \tfrac{1}{2}\ \tan^{-1}\ \frac{2(\alpha_{12}\alpha_{22}+\beta^2\alpha_{11}\alpha_{21})}{(\alpha_{12}^2-\alpha_{22}^2)+\beta^2(\alpha_{11}^2-\alpha_{21}^2)} \quad \text{----------------}(3\text{-}45)$$

$$\phi\ \ = \tfrac{1}{2}\ \tan^{-1}\ \frac{2(\alpha_{11}\alpha_{12}+\frac{\beta^2}{\theta^4}\alpha_{21}\alpha_{22})}{(\alpha_{12}^2-\alpha_{11}^2)+\frac{\beta^2}{\theta^4}(\alpha_{22}^2-\alpha_{21}^2)} \quad \text{----------------}(3\text{-}46)$$

By use of the relations 3-27 and 3-31, and the relation det T_α = 1 the equations 3-43 and 3-44 become

$$y_{p+\frac{1}{2}}^2 + \frac{\dot{y}_{p+\frac{1}{2}}^2}{\frac{\theta^4}{\beta^2}} = \frac{x_0^2+\beta^2\dot{x}_0^2}{\theta^2} \qquad \text{------------------------(3-47)}$$

and

$$x_{p+\frac{1}{2}}^2 + \frac{\dot{x}_{p+\frac{1}{2}}^2}{\frac{1}{\beta^2}} = \theta^2(y_0^2+\frac{\beta^2}{\theta^4}\dot{y}_0^2) \qquad \text{------------------------(3-48)}$$

and

$$\phi_x = 90^\circ, \ \phi_y = 90^\circ$$

Now from 3-41 and 3-42 it is seen that corresponding to each set of $(x_p, \dot{x}_p)$ and $(y_p, \dot{y}_p)$ there corresponds a whole family of sets $(x_0, \dot{x}_0)$ and $(\dot{y}_0, y_0)$. The limiting two families of sets $(x_0, \dot{x}_0)$ and $(y_0, \dot{y}_0)$ correspond to the boundary conditions $(x_{pmax}, 0)$ and $(y_{pmax}, 0)$ and are consequently given by the relation

$$\frac{x_0^2}{x_{pmax}^2} + \frac{\dot{x}_0^2}{\frac{x_{pmax}^2}{\beta}} = 1 \qquad \text{-----------------------------(3-49)}$$

and

$$\frac{y_0^2}{y_{pmax}^2} + \frac{\dot{y}_0^2}{\left(\frac{\theta^2 y_{pmax}}{\beta}\right)^2} = 1 \qquad \text{------------------------(3-50)}$$

The above two equations represent two ellipses in the phase space $(x_0,\dot{x}_0)$ and $(y_0,\dot{y}_0)$ respectively. Any particle whose initial $(x_0,\dot{x}_0)$ coordinates lie within the ellipse defined by the equation 3-49 will be transmitted through the accelerator such that the x-coordinates at the end of any repeat section will always satisfy

$$x < x_{pmax}$$

Similarly, any particle whose initial $(y_0,\dot{y}_0)$ coordinates lie within the ellipse defined by equation 3-50 will be transmitted through the accelerator such that the particle's y-coordinate at the end of any repeat section will always satisfy

$$y < y_{pmax}$$

Similarly, from 3-47 and 3-48 one obtains

$$\frac{x_0^2}{(\theta\ y_{p+\frac{1}{2}max})^2} + \frac{\dot{x}_0^2}{\left(\frac{\theta\ y_{p+\frac{1}{2}max}}{\beta}\right)^2} = 1 \text{ --------------------------- } (3\text{-}51)$$

and

$$\frac{y_0^2}{\left(\frac{x_{p+\frac{1}{2}max}}{\theta}\right)^2} + \frac{\dot{y}_0^2}{\left(\frac{\theta \ x_{p+\frac{1}{2}max}}{\beta}\right)^2} = 1 \quad \text{------------------------(3-52)}$$

where $x_{p+\frac{1}{2}max}$ and $y_{p+\frac{1}{2}max}$ are the maximum excursions at the middle of any repeat section and in the horizontal and the vertical planes respectively. Here again the two ellipses in the $(x_0,\dot{x}_0)$ and $(y_0,\dot{y}_0)$ planes define the limiting injection parameters such that no particles exceed $x_{p+\frac{1}{2}max}$ and $y_{p+\frac{1}{2}max}$ at the middle of any repeat section. Now, it is customary to define the acceptance of an accelerator in any given phase space, for instance x_0,x_0, as $1/\Pi$ times the area of the corresponding limiting ellipse.

Thus, the acceptance at the entrance to the accelerator and in the vertical plane is

$$A_{x_0} = \frac{1}{\Pi}\left(\Pi \ x_{pmax} \ \frac{x_{pmax}}{\beta}\right)$$

$$= \frac{(x_{pmax})^2}{\beta}$$

$$= \frac{(\theta \ y_{p+\frac{1}{2}max})^2}{\beta} \quad \text{---------------------------------(3-53)}$$

Similarly, the acceptance at the accelerator entrance and in the horizontal plane is

$$A_{y_0} = \frac{(\theta \; y_{pmax})^2}{\beta}$$

$$= \frac{(x_{p+\frac{1}{2}max})^2}{\beta} \qquad \text{------------------------------------(3-54)}$$

From 3-53 and 3-54 one obtains

$$x_{pmax} = \theta \; y_{p+\frac{1}{2}max} \qquad \text{------------------------------------(3-55)}$$

and

$$y_{pmax} = \frac{x_{p+\frac{1}{2}max}}{\theta} \qquad \text{------------------------------------(3-56)}$$

Now from Fig. 2-4 of section 2-4 it may be seen that the vertical motion of a particle will take place alternately in focusing and defocusing planes. Similarly the horizontal motion will take place alternately in the defocusing and the focusing planes. It is evident from Liouville's Theorem that the phase space acceptance for vertical motion at the entrance of the accelerator and in the focusing plane is equal in magnitude to the phase space acceptance for vertical motion one half repeat section later and in the defocusing plane. A similar conservation of phase space acceptance holds for motion in the horizontal plane. In view of this and because the

structure is assumed to be periodic, it follows that the acceptance at the entrance to the accelerator has the same magnitude for horizontal and vertical motion respectively, i.e.,

$$A_{x_0} = A_{y_0} \qquad \text{(3-57)}$$

Thus, using the equations 3-53 and 3-54 in 3-57 one obtains

$$x_{pmax} = \theta\, y_{p+\frac{1}{2}max} = \theta\, y_{pmax} = x_{p+\frac{1}{2}max} \qquad \text{(3-58)}$$

Now using the boundary condition that

$$x_{pmax} = b$$

and the relation 3-58 the equations 3-49, 3-50, 3-51, and 3-52 become

$$\frac{x_0^2}{b^2} + \frac{\dot{x}_0^2}{\left(\frac{b}{\beta}\right)^2} = 1 \qquad \text{(3-59)}$$

and

$$\frac{y_0^2}{\left(\frac{b}{\theta}\right)^2} + \frac{\dot{y}_0^2}{\left(\frac{b}{\beta}\theta\right)^2} = 1 \qquad \text{(3-60)}$$

The ellipses described by the equations 3-59 and 3-60 are shown in Fig. 3-1 below

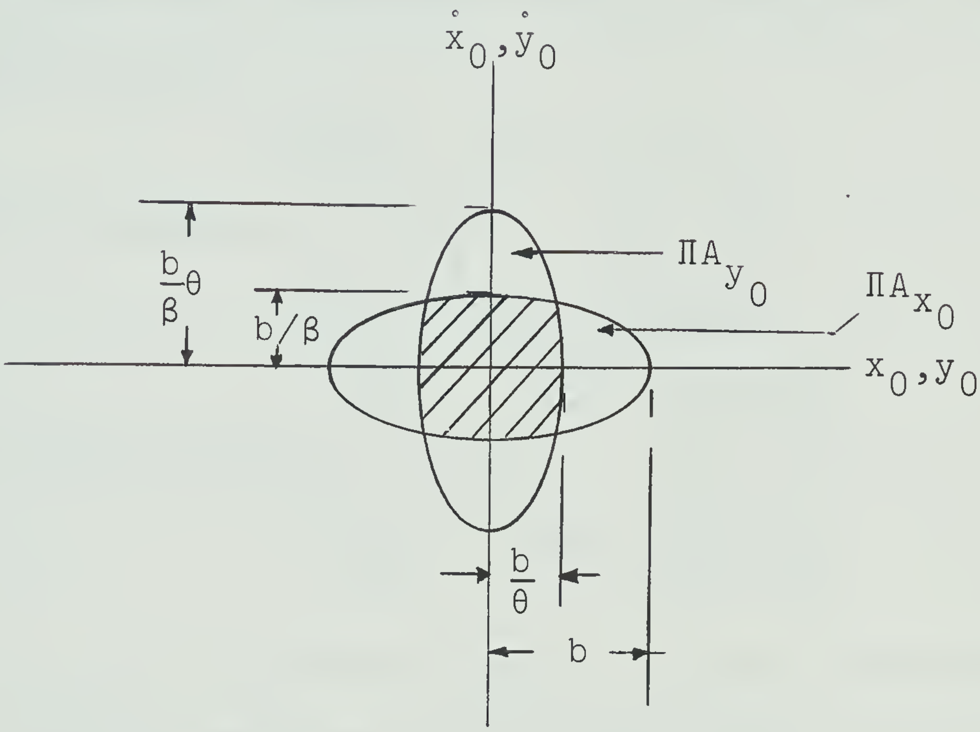

Fig. 3-1 Transverse Acceptance at the Plane of Injection of an Accelerator with Identical Repeat Sections

Now, a cylindrically symmetric beam is identical to itself if rotated through 90° about its axis. Thus the phase space emittance of the particle beam in the focusing plane is congruent with that in the defocusing plane. From this it follows that only that part of the emittance common to both the ellipses of Fig. 3-1 is accepted and therefore the transverse acceptance at the plane of injection is $\frac{1}{\Pi}$ times the shaded area.

The transverse acceptance at any other plane can also be found as follows:

The equations in matrix form between the plane of injection and any other transverse plane, denoted by suffix 1, can be written as

for vertical motion $$\begin{pmatrix} x_1 \\ \dot{x}_1 \end{pmatrix} = \begin{pmatrix} a_1 & b_1 \\ c_1 & d_1 \end{pmatrix} \begin{pmatrix} x_0 \\ \dot{x}_0 \end{pmatrix} \quad \text{---------(3-61)}$$

for horizontal motion $$\begin{pmatrix} y_1 \\ \dot{y}_1 \end{pmatrix} = \begin{pmatrix} a_2 & b_2 \\ c_2 & d_2 \end{pmatrix} \begin{pmatrix} y_0 \\ \dot{y}_0 \end{pmatrix} \quad \text{--------(3-62)}$$

where a_1, b_1, c_1, d_1 and a_2, b_2, c_2, d_2 are the elements of the transfer matrices for vertical and horizontal planes respectively.

Using the relations $a_1 d_1 - b_1 c_1 = 1$ and $a_2 d_2 - b_2 c_2 = 1$ the foregoing equations become

$$\begin{pmatrix} x_0 \\ \dot{x}_0 \end{pmatrix} = \begin{pmatrix} d_1 & -b_1 \\ -c_1 & a_1 \end{pmatrix} \begin{pmatrix} x_1 \\ \dot{x}_1 \end{pmatrix} \quad \text{----------------------------(3-63)}$$

$$\begin{pmatrix} y_0 \\ \dot{y}_0 \end{pmatrix} = \begin{pmatrix} d_2 & -b_2 \\ -c_2 & a_2 \end{pmatrix} \begin{pmatrix} y_1 \\ \dot{y}_1 \end{pmatrix} \quad \text{----------------------------(3-64)}$$

Using the boundary values of $(x_0, \dot{x}_0)$ and $(y_0, \dot{y}_0)$ given by equations 3-59 and 3-60 the above equations become

$$\frac{(d_1x_1-b_1\dot{x}_1)^2}{b^2}+\frac{(a_1\dot{x}_1-c_1x_1)^2}{\left(\frac{b}{\beta}\right)^2}=1 \text{ ------------------}(3\text{-}65)$$

$$\frac{(d_2y_1+b_2\dot{y}_1)^2}{\left(\frac{b}{\theta}\right)^2}+\frac{(a_2\dot{y}_1-c_2y_1)^2}{\left(\frac{b\theta}{\beta}\right)^2}=1 \text{ ------------------}(3\text{-}66)$$

By rotation of axes the foregoing equations can be written as

$$\frac{x^2}{A^2b^2}+\frac{x^2}{B^2b^2}=1 \text{ ----------------------------------}(3\text{-}67)$$

$$\frac{y^2}{C^2\left(\frac{b}{\theta}\right)^2}+\frac{\dot{y}^2}{D^2\left(\frac{b}{\theta}\right)^2}=1 \text{ ------------------------------}(3\text{-}68)$$

where

$$A=1/\sqrt{(d_1^2+c_1^2\beta^2)\mathrm{COS}^2\phi_x+(b_1^2+a_1^2\beta^2)\mathrm{SIN}^2\phi_x-2(d_1b_1+c_1a_1\beta^2)\mathrm{SIN}\ \phi_x\mathrm{COS}\ \phi_x}$$

$$B=1/\sqrt{(b_1^2+a_1^2\beta^2)\mathrm{COS}^2\phi_x-(d_1^2+c_1^2\beta^2)\mathrm{SIN}^2\phi_x+2(d_1b_1+c_1a_1\beta^2)\mathrm{SIN}\ \phi_x\mathrm{COS}\ \phi_x}$$

$$C=1/\sqrt{(d_2^2+\frac{c_2^2\beta^2}{\theta^4})\mathrm{COS}^2\phi_y+(b_2^2+\frac{a_2^2\beta^2}{\theta^4})\mathrm{SIN}^2\phi_y-2(d_2b_2+\frac{c_2a_2\beta^2}{\theta^4})\mathrm{SIN}\ \phi_y\mathrm{COS}\ \phi_y}$$

$$D=1/\sqrt{}(b_2^2+\frac{a_2^2\beta^2}{\theta^4})\mathrm{COS}^2\phi_y-(d_2^2+\frac{c_2^2\beta^2}{\theta^4})\mathrm{SIN}^2\phi_y+2(d_2b_2+\frac{c_2a_2\beta^2}{\theta^4})\mathrm{SIN}\ \phi_y\mathrm{COS}\ \phi_y$$

and where the axes have been rotated by angles ϕ_x and ϕ_y given by

$$\phi_x = \frac{1}{2}\tan^{-1}\left\{2(b_1d_1+c_1a_1\beta^2)/((b_1^2-d_1^2)+\beta^2(a_1^2-c_1^2))\right\}$$

$$\phi_y = \frac{1}{2}\tan^{-1}\left\{2(b_2d_2+\frac{c_2a_2\beta^2}{\theta^4})/((b_2^2-d_2^2)+\frac{\beta^2}{\theta^4}(a_2^2-c_2^2))\right\}$$

Equations 3-65 and 3-66 are shown in Fig. 3-2 where the acceptance at the transverse plane denoted by subscript 1 is the shaded area common to both ellipses.

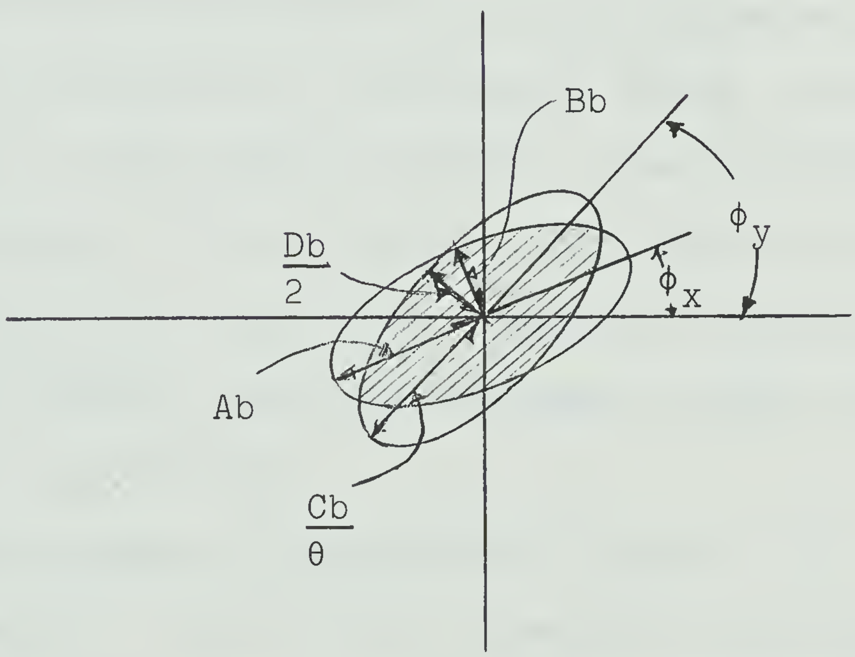

Fig. 3-2 Transverse Acceptance at any Plane Along the Accelerator

CHAPTER 4

NUMERICAL STUDIES OF THE MICROPARTICLE DYNAMICS IN LINEAR PARTICLE ACCELERATOR

4.1 Introduction

In Chapter 2 of this thesis the basic formulas of the particle motion in the accelerator sections and in quadrupole lenses were derived. The results of this study were applied in Chapter 3 to investigate the properties of particle motion in the transverse planes of an idealized accelerator structure in which all sections are identical. The study of Chapter 3 has neglected any velocity gain of the particles, and for this reason the approach that has been used, while providing useful physical insight cannot be employed to make exact numerical calculations.

The purpose of the present chapter is to make an exact computer study of the dynamics of particles in an accelerator structure. The formulas used here are those that have been derived in Chapter 2.

4.2 The Computer Program

4.2.1 General Discussion

A program has been written for the IBM System/360 computer. The purpose of the program is to design the accelerator drift tube structure for a given set of nominal particle input parameters. These nominal input parameters are the particle charge to mass ratio, its injection potential, its synchronous phase, the operating frequency, the peak voltage in the gap, the radius of the drift tubes, and the ratio of the gap length to the drift tube length. Once the structure has been designed, its properties are then studies while the input conditions are varied about their nominal values. This study for varying input conditions is conducted first without, and then with quadrupole focusing elements within the above designed structure. The results are obtained partially in tabular form and partially in graphical form. They are presented throughout the remainder of this chapter.

4.2.2 Function of the Program

The dimensions of an accelerator structure without quadrupoles as shown in fig. 4.1 are computed in the subroutine STRUCT for a synchronous particle running along

the axis of the accelerator. This subroutine can also be used for designing the structure for an off axis synchronous particle although this has not been done in this work. Subroutine STRUCT also computes the synchronous velocity and the synchronous energy at the various drift tube centres.

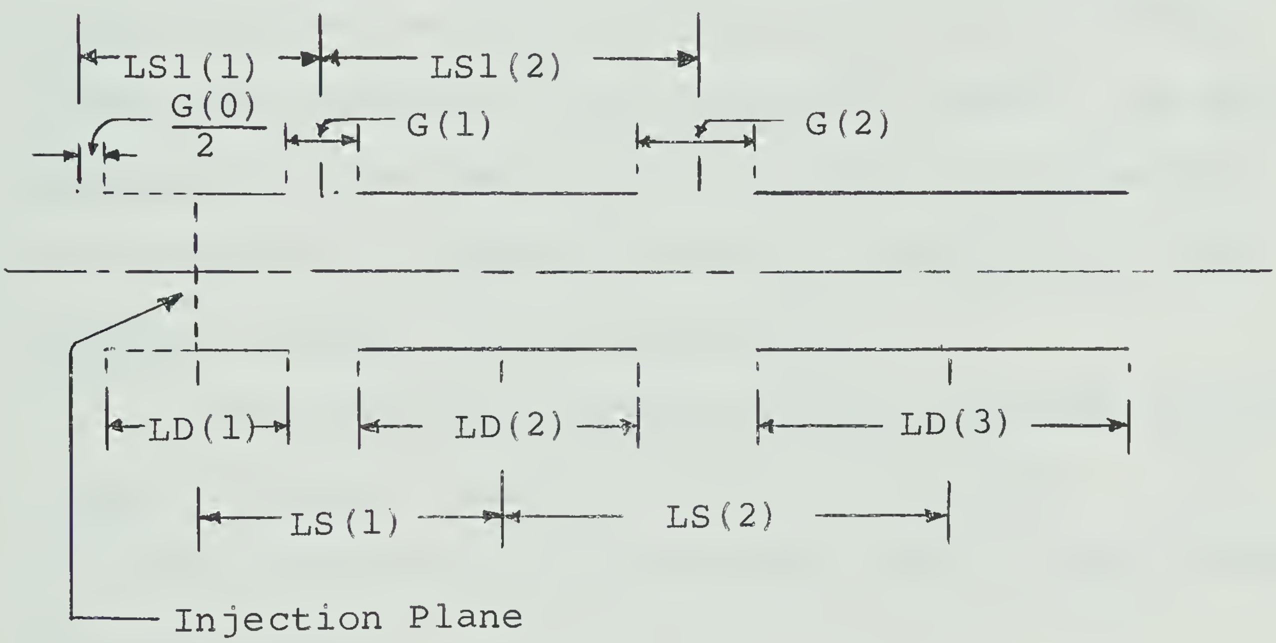

Note: The same symbols are used in the program

Fig. 4.1 The First Two Sections of the Accelerator

The main program is divided into two parts. The first part is for the structure without quadrupoles and the second part with quadrupoles. However, the

second part can also be used for the structure without quadrupoles if one takes the quadrupole voltage to be equal to zero.

The subroutine RESULT uses the dimensions found by STRUCT to compute the velocity gain, energy gain, change in particle phase for a given section for nonsynchronous particles. Further the subroutine RESULT computes the change in slope of each particle trajectory at the centre of the gap in that section. Using the findings of the subroutine RESULT, the main program now computes the actual particle trajectory. This process is repeated section by section for the complete length of the accelerator.

The subroutine PLOTNG produces different graphs from the digital output of the main program. A list of identification of the variables used in the program is given below.

Program Variables	Identification of the Variables
A	Inner radius of the drift tubes in meters
ALPHA(N)	Same as k_n in equation 2-4 of page 8
ANGL	Angle in radians
BI1	$I_o(\Pi r/LS_n)$
BI2	$I_o(\Pi a/LS_n)$

Program Variables	Identification of the Variables
BI3	$I_1(\Pi r/LS_n)$
BI4	$I_2(\Pi r/LS_n)$
B15	$I_1(\Pi a/LS_n)$
BESI	Library subroutine for the Bessel functions
D	Distance of the quadrupole tips from the axis of the accelerator in meters
DEG	The projections of the angle of the trajectory at injection in degrees on both horizontal and vertical planes.
DELTA	Same as Δ_n in equation 2-13 of page 12 for synchronous particle
DELTA1	Same as Δ_n in equation 2-13 of page 12 for nonsynchronous particle
DELV	Velocity gain in Meters/Sec. for a nonsynchronous particle in one section
DELVS	Velocity gain in Meters/Sec. for a synchronous particle in one section
DENERG(N)	Difference between the synchronous and the nonsynchronous energy in volts at the middle of the nth drift tube
DENG	Energy gain in volts for a nonsynchronous particle in the nth section

Program Variables	Identification of the Variables
DENGY	Energy gain in volts for a synchronous particle in the nth section
DPHI(N+1)	Difference between the nonsynchronous and the synchronous phase in degrees at the nth gap centre.
DX, DXPR, DX1	Change in transverse velocity in meters/sec. in the vertical plane and at the gap centres
DY, DYPR, DY1	Change in transverse velocity in meters/sec. in the horizontal plane and at the gap centres
EM	Charge to mass ratio in coulombs/Kg
ENERGS(N)	Energy of the synchronous particle in volts at the middle of the nth drift tube
ENERGY(N)	Energy of the nonsynchronous particle in volts at the middle of the nth drift tube
F	Operating frequency in cycles/sec
FA	Ratio of the axial length of the quadrupoles to the drift tube length
FB	Ratio of the gap length to the drift tube length
G(N)	Length of the nth gap in meters

Program Variables	Identification of the Variables
IK	Dummy variable
IERI, IER2, IER3, IER4, IER5	Error Codes
J2(N)	An array of data points to be plotted for graphs
L	Number of drift tubes
LS1, SS2	Distance in meters from the (n-1)th gap centre to the nth gap centre
LD(N)	Length of the nth drift tube in meters
LS(N)	Length of the nth section in meters
M	A variable which determines the symbols to be used in the graphs
NA	Total number of points to be plotted in the graph
PH	Nonsynchronous phase in degrees at the middle of the first drift tube
PHI(1), PHIS(1)	Nonsynchronous and synchronous phase in radians at the middle of the 1st drift tube
PHIS(N+1)	Synchronous phase in radians at the nth gap centre
PHI(N+1)	Nonsynchronous phase in radians at the nth gap centre
PHS, PHIS1(N)	Synchronous phase in degrees at the nth gap centre

Program Variables	Identification of the Variables
P1	Same as k defined in equation 2-25 of page 21
Q1, Q11, Q12	The arguments of COS, COSH, SIN, SINH of equations 2-34 and 2-35 of page 23 and 24 respectively
R(N)	Radial excursion in meters at the middle of the nth drift tube
R1	Radial excursion in meters at the gap centre
RPRIME(N)	Radial velocity of the particle in meters/sec. at the middle of the nth drift tube
RPRIM6	Average radial velocity in meters/sec. at the gap
S, SA, S3, S4, S5, S6, TS, TS1, TS2	The times taken by the particle in transversing different portions of an accelerator section
TOTLEN	Total length of the structure in meters
TT(N)	Transit time factor for the particle at synchronous velocity
VS(N)	Synchronous velocity in meters/sec. at the middle of the nth drift tube
V(N)	Nonsynchronous velocity in meters/sec. at the middle of the nth drift tube

Program Variables	Identification of the Variables
VM	Peak voltage in the gaps in volts
VM1	Voltage of the particle at injection in volts
VM2	Voltage between the adjacent quadrupoles in volts
V2(N)	Error in the computation of the length LS1(N)
W	Same as Q in equation 2-29 of page 21
X(N)	Transverse excursion in meters in the vertical plane and at the middle of the nth drift tube
XA, X1, X2, X3, X4, X5, X6	Transverse excursions in meters in the vertical plane and at different cross-sections within an accelerator section
XPRIME(N)	Transverse velocity in meters/sec. in the vertical plane and at the middle of the nth drift tube
XPRIM1, XPRIM2, XPRIM3, XPRIM4, XPRIM5, XPRIM6	Transverse velocity in meters/sec in the vertical plane and at different cross-sections within an accelerator section

Program Variables	Identification of the Variables
Y(N) YA, Y1, Y2, Y3, Y4, Y5, Y6, YPRIM1, YPRIM2, YPRIM3 YPRIM4, YPRIM5, YPRIM6	Same as X(N), XA, X1, etc. described above but in the horizontal plane

4.2.3 Flow Charts

MAIN PROGRAM

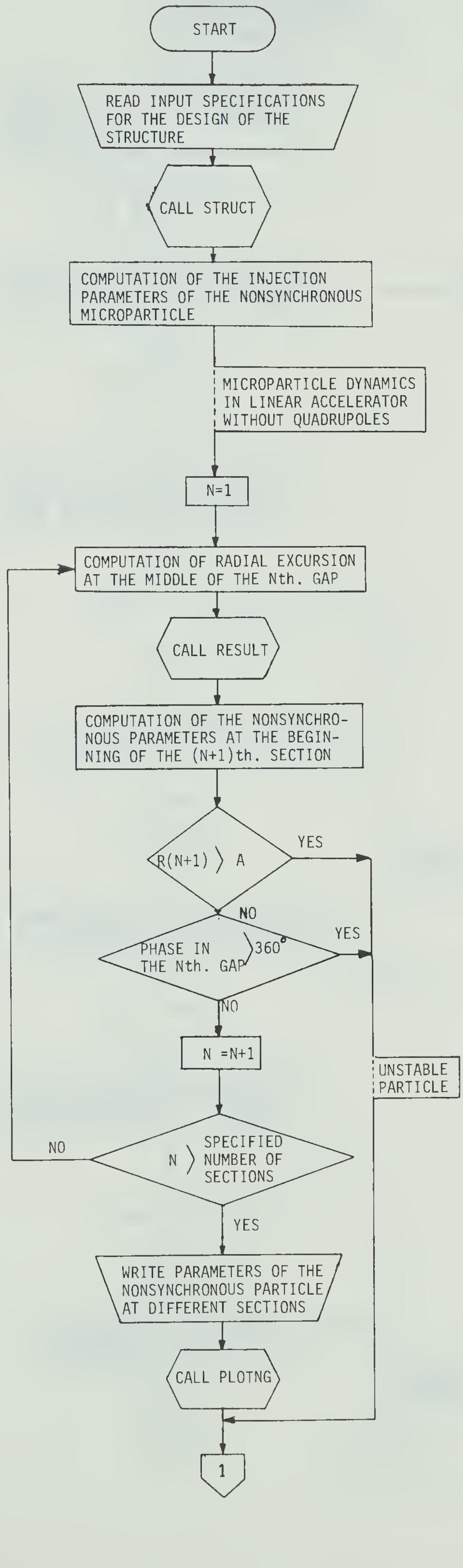

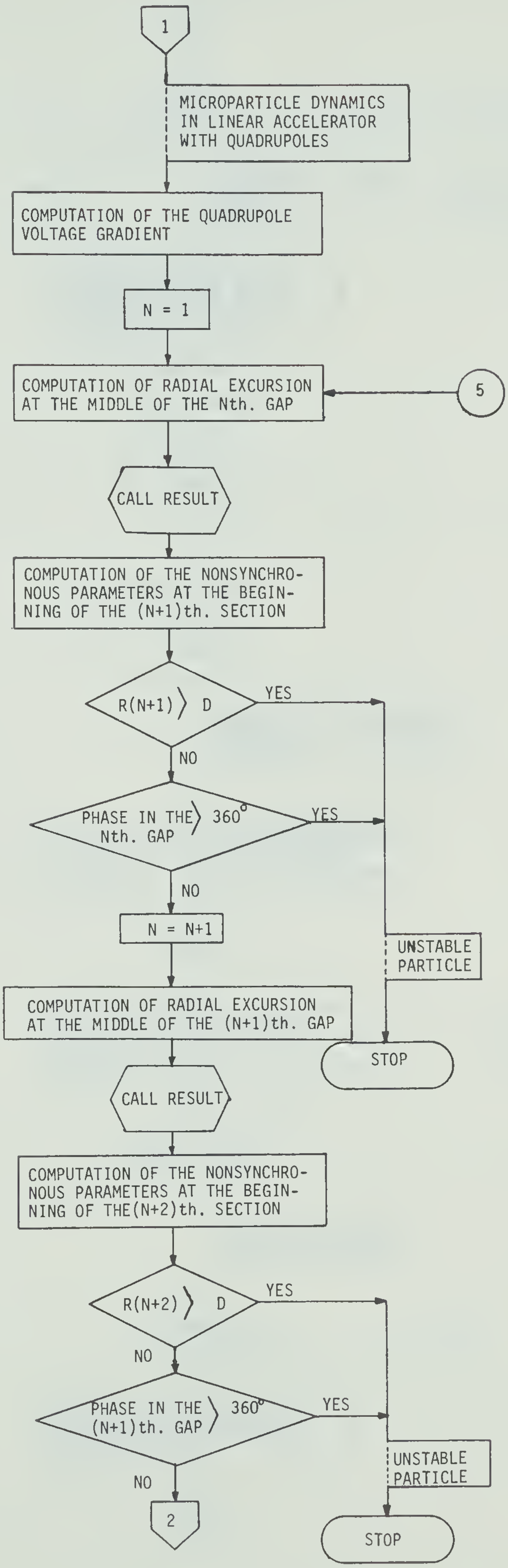
1
MICROPARTICLE DYNAMICS IN LINEAR ACCELERATOR WITH QUADRUPOLES
COMPUTATION OF THE QUADRUPOLE VOLTAGE GRADIENT
N = 1
COMPUTATION OF RADIAL EXCURSION AT THE MIDDLE OF THE Nth. GAP
5
CALL RESULT
COMPUTATION OF THE NONSYNCHRONOUS PARAMETERS AT THE BEGINNING OF THE (N+1)th. SECTION
R(N+1) 〉 D
YES
NO
PHASE IN THE Nth. GAP 〉 360°
YES
NO
N = N+1
UNSTABLE PARTICLE
COMPUTATION OF RADIAL EXCURSION AT THE MIDDLE OF THE (N+1)th. GAP
STOP
CALL RESULT
COMPUTATION OF THE NONSYNCHRONOUS PARAMETERS AT THE BEGINNING OF THE(N+2)th. SECTION
R(N+2) 〉 D
YES
NO
PHASE IN THE (N+1)th. GAP 〉 360°
YES
NO
UNSTABLE PARTICLE
2
STOP

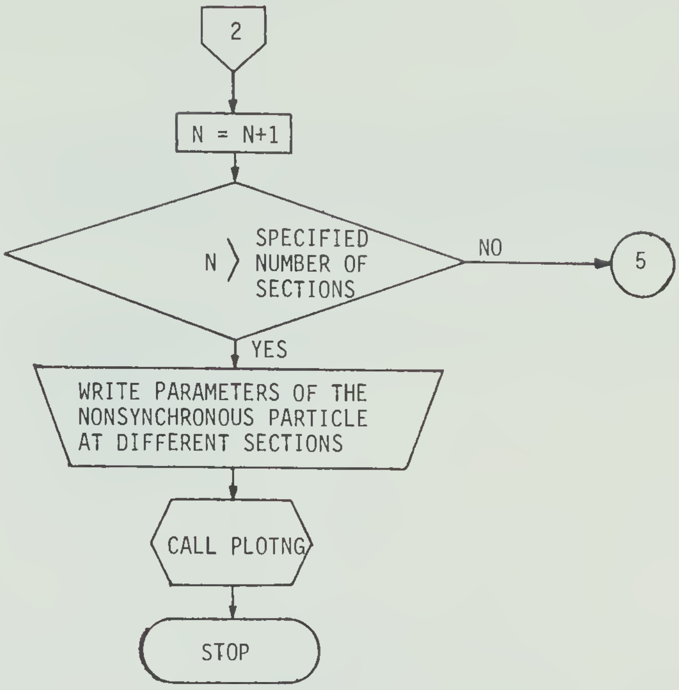

SUBROUTINE STRUCT

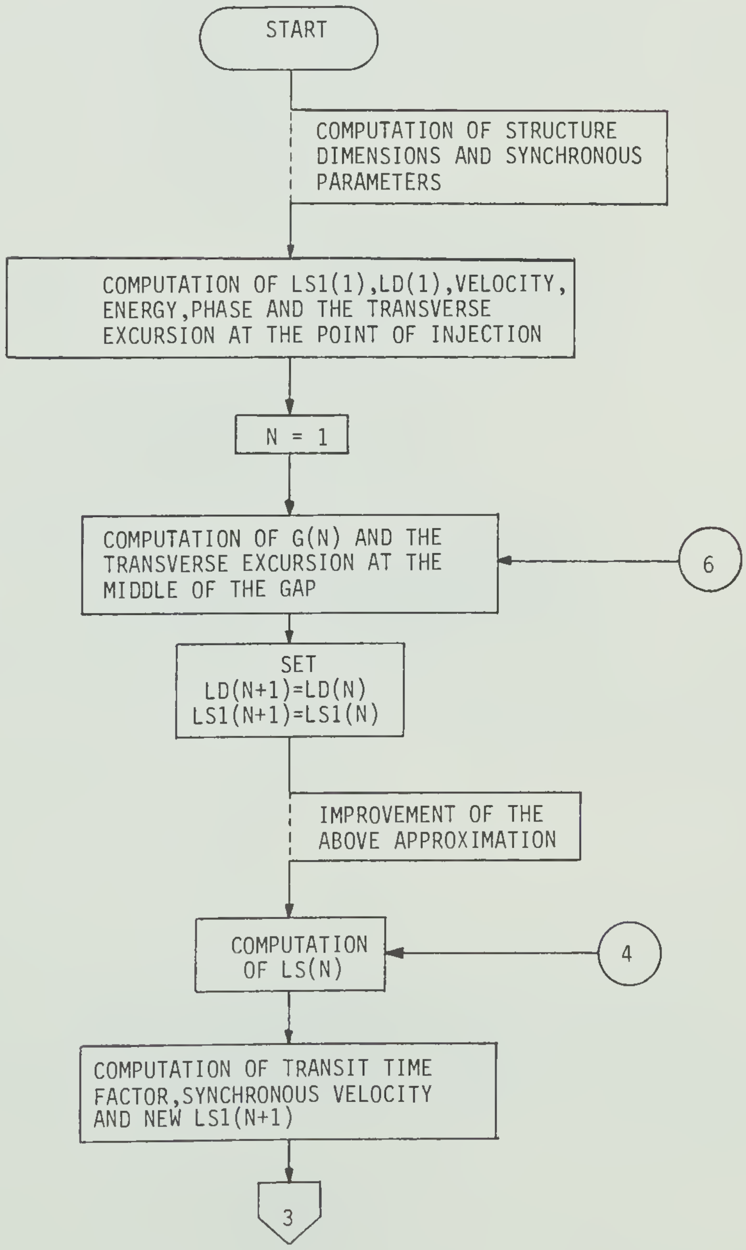

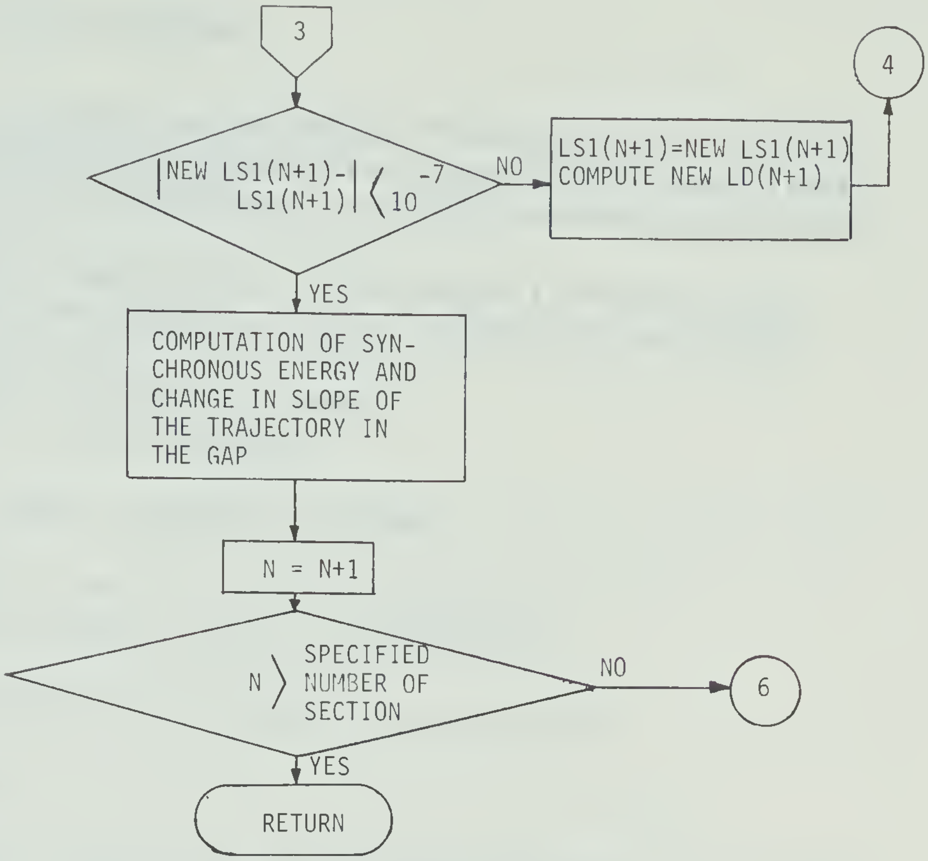

SUBROUTINE RESULT

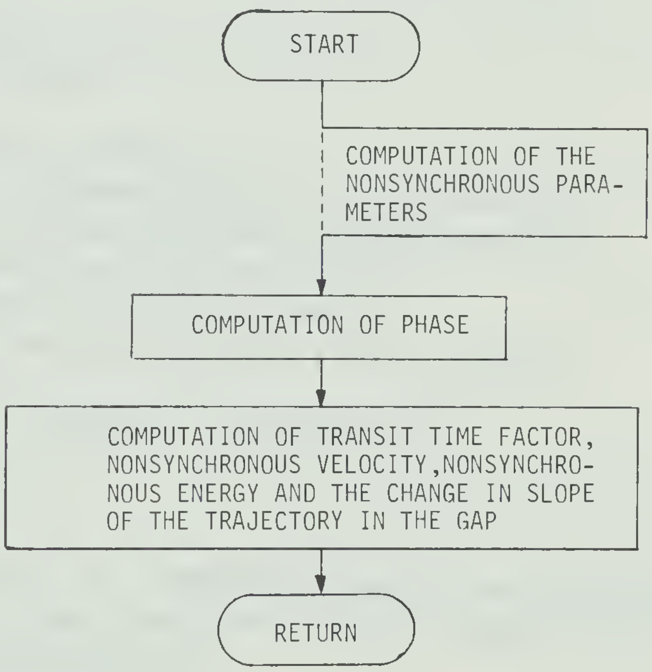

SUBROUTINE PLOTNG

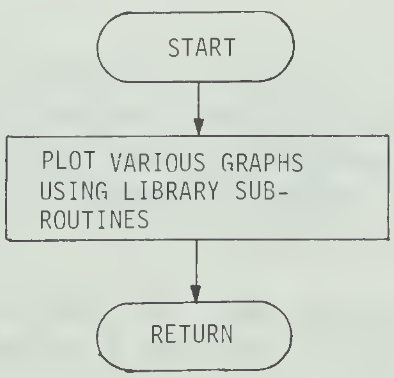

4.2.4 Listing of the Program

```
      COMMON EM,VM1,F,R1,A,VM,L,FB,PH,DELTA1,LS(40),
     1G(40),ENERGS(40),ENERGY(40),DVEL(40),DPHI(40),
     1VS(40),LD(40),PHIS(40),PHI(40),ALPHA(40),V(40),
     1DENERG(40)
      DIMENSION X(40),Y(40),XPRIME(40),YPRIME(40),
     1XPRIM(40),YPRIM(40),R(40),J2(40),DATA(1024)
      REAL LD,LS,J2
      CALL PLOTS (DATA(1) ,4096)
      CALL PLOT (0.0,3.0,23)

      NOMINAL INPUT SPECIFICATIONS

      READ(5,40)A,VM,VM1,F,EM,L,D,FA,FB
   40 FORMAT(F5.2,3F9.1,F6.1,I2,3F5.3)

      COMPUTATION OF STRUCTURE DIMENSIONS

      CALL STRUCT

      INJECTION PARAMETERS OF NONSYNCHRONOUS PARTICLE
      AT THE MIDDLE OF FIRST DRIFT TUBE

      READ(5,5)X(1),Y(1),DEG,PH
    5 FORMAT(4F10.5)
      M=130
      V(1)=SQRT(2.*EM*VM1)
      XPRIME(1)=(TAN(DEG/57.29582))*V(1)
      YPRIME(1)=(TAN(DEG/57.29582))*V(1)
      ENERGY(1)=.5*( V(1)**2.)/EM
      PHI(1)=(-90.+PH)/57.29582
      DPHI(1)=(PHI(1)-PHIS(1))*57.29582

      STRUCTURE WITHOUT QUADRUPOLES

      DO 80 N=1,L

      COMPUTATION OF NONSYNCHRONOUS PARAMETERS AT
      THE MIDDLE OF (N+1)TH. DRIFT TUBE FOR STRUCTURE
      WITHOUT QUADRUPOLES

      J2(N)=FLOAT(N)
      NA=N

      FOR THE COMPUTATION OF PARTICLE TRAJECTORY,
      EACH SECTION HAS BEEN DIVIDED INTO SEVERAL
      SUB-SECTIONS. THESE SUB-SECTIONS ARE DEFINED
      IN THE FOLLOWING COMMENTS WHERE THE DESCRIPTION
      OF S4,S5,TS,S,S3,TS1,SA,S31,TS2 IS ALSO GIVEN

      S4 IS THE TIME TAKEN BY THE PARTICLE TO
      TRAVERSE THE LENGTH FROM THE CENTRE OF THE NTH.
```

```
   DRIFT TUBE TO THE CENTRE OF THE NTH. GAP

   S4=.5*(1.+FB)*LD(N)/V(N)
   XA=X(N)+S4*XPRIME(N)
   YA=Y(N)+S4*YPRIME(N)
   R1 =SQRT((XA**2)+(YA**2))
   XPRIM1=XPRIME(N)
   YPRIM1=YPRIME(N)
   CALL RESULT(N,XPRIM1,YPRIM1,XA,YA,DXPR,DYPR)
   XPRIME(N+1)=XPRIME(N)+DXPR
   YPRIME(N+1)=YPRIME(N)+DYPR

   S5 IS THE TIME TAKEN BY THE PARTICLE TO TRAVERSE
   THE LENGTH FROM THE CENTRE OF THE NTH. GAP TO
   THE CENTRE OF THE (N+1)TH. DRIFT TUBE

   S5=((.5*LD(N+1))+(.5*G(N)))/( V(N+1))
   X(N+1)=XA+S5*XPRIME(N+1)
   Y(N+1)=YA+S5*YPRIME(N+1)
   XPRIM(N)=(ATAN(XPRIME(N)/V(N)))*57.29582
   YPRIM(N)=(ATAN(YPRIME(N)/V(N)))*57.29582
   R(N+1)=SQRT((X(N+1)**2)+(Y(N+1)**2))
   IF((R(N+1)) .GT.  A ) GO TO 7
   IF(ABS(PHI(N+1)) .GT. 6.28318) GO TO 7
80 CONTINUE

   OUTPUT IN TABULAR FORM

7  WRITE(6,25)((K,X(K),Y(K),DPHI(K),DVEL(K),DENERG(K)),
  1K=1,NA)
25 FORMAT((5X,I2,5(5X,F11.4)))

   OUTPUT IN GRAPHICAL FORM

   CALL PLOTNG (J2,NA,X,Y,L,M )

   STRUCTURE WITH AND WITHOUT QUADRUPOLES

   COMPUTATION OF FIELD GRADIENT FOR QUADRUPOLE
   VOLTAGE VM2. FOR STRUCTURE WITHOUT QUADRUPOLES
   SET VM2=0.

   READ(5,45)VM2
45 FORMAT(F10.2)
   P1= VM2/(D**2.)
   W=SQRT(P1*(EM))
   DO 89 N=1,L,2

   COMPUTATION OF NONSYNCHRONOUS PARAMETERS AT THE
   MIDDLE OF (N+1)TH. AND (N+2)TH. DRIFT TUBES FOR
   THE STRUCTURE WITH AND WITHOUT QUADRUPOLES

   J2(N)=FLOAT(N)
   NA=N

   TS IS THE TIME TAKEN BY THE PARTICLE TO TRAVERSE
   THE SECOND HALF LENGTH OF THE QUADRUPOLES IN
```

```
      THE NTH. DRIFT TUBE

      TS=(FA*LD(N))/(V(N)*2.)
      Q1=W*TS
      Q2=COSH(Q1)
      Q3=SINH(Q1)
      Q4=COS(Q1)
      Q5=SIN(Q1)
      IF(W .EQ. 0.) GO TO 26
      Q6=Q5/W
      Q7=Q3/W
      GO TO 27

      THE FOLLOWING THREE STATEMENTS ARE USED FOR
      STRUCTURE WITHOUT QUADRUPOLES

   26 Q6=FA*LD(N)/(2.*V(N))
      Q6=Q7
      D=A
   27 X1=(X(N)*Q4)+( XPRIME(N)*Q6)
      XPRIM1=-(X(N)*Q5*W)+(XPRIME(N)*Q4)
      Y1=(Y(N)*Q2)+( YPRIME(N)*Q7)
      YPRIM1=(Y(N)*Q3*W)+(YPRIME(N)*Q2)

      S IS THE TIME TAKEN BY THE PARTICLE TO TRAVERSE
      THE LENGTH FROM THE END OF THE QUADRUPOLES IN
      THE NTH. DRIFT TUBE TO THE CENTRE OF THE NTH. GAP

      S=(G(N)+((1.-FA)*LD(N)))/(2.*V(N))
      X2=X1+(S*XPRIM1)
      Y2=Y1+(S*YPRIM1)
      R1=SQRT((ABS(X2))**2 +(ABS(Y2))**2 )
      CALL RESULT(N,XPRIM1,YPRIM1,X2,Y2,DX,DY)
      XPRIM2=XPRIM1+DX
      YPRIM2=YPRIM1+DY

      S3 IS THE TIME TAKEN BY THE PARTICLE TO TRAVERSE
      THE LENGTH FROM THE CENTRE OF THE NTH. GAP TO
      THE BEGINNING OF THE QUADRUPOLES IN THE (N+1)TH.
      DRIFT TUBE

      S3=(G(N)+((1.-FA)*LD(N+1)))/(2.*V(N+1))
      X3=X2+(S3*XPRIM2)
      Y3=Y2+(S3*YPRIM2)

      TS1 IS THE TIME TAKEN BY THE PARTICLE TO TRAVERSE
      THE FIRST HALF LENGTH OF THE QUADRUPOLES IN THE
      (N+1)TH. DRIFT TUBE. THIS IS ALSO THE TIME TAKEN
      BY THE PARTICLE TO TRAVERSE THE SECOND HALF
      LENGTH OF THE (N+1)TH. QUADRUPOLES

      TS1=((FA*LD(N+1))/(V(N+1)*2.))
      Q11=W*TS1
      Q21=COSH(Q11)
      Q31=SINH(Q11)
      Q41=COS(Q11)
      Q51=SIN(Q11)
```

```
      IF(W .EQ. 0.) GO TO 28
      Q61=Q51/W
      Q71=Q31/W
      GO TO 29

      THE FOLLOWING TWO STATEMENTS ARE USED FOR
      STRUCTURE WITHOUT QUADRUPOLES

   28 Q61=FA*LD(N+1)/(2.*V(N+1))
      Q71=Q61
   29 X(N+1)=(X3*Q21)+( XPRIM2*Q71)
      XPRIME(N+1)= (X3*Q31*W)+(XPRIM2*Q21)
      XPRIM(N+1)=(ATAN(XPRIME(N+1)/V(N+1)))*57.29582
      Y(N+1)=(Y3*Q41)+(YPRIM2*Q61 )
      R(N+1)=SQRT((X(N+1)**2)+(Y(N+1)**2))
      IF((R(N+1)) .GT.  D ) GO TO 15
      IF(ABS(PHI(N+1)) .GT. 6.28318) GO TO 15
      YPRIME(N+1)=-(Y3*Q51*W)+(YPRIM2*Q41)
      YPRIM(N+1)=(ATAN(YPRIME(N+1)/V(N+1)))*57.29582
      X4=X(N+1)*Q21+XPRIME(N+1)*Q71
      XPRIM4=(X(N+1)*Q31*W)+(XPRIME(N+1)*Q21)
      Y4=(Y(N+1)*Q41)+(YPRIME(N+1)*Q61)
      YPRIM4=-(Y(N+1)*Q51*W)+(YPRIME(N+1)*Q41)

      SA IS THE TIME TAKEN BY THE PARTICLE TO TRAVERSE
      THE DISTANCE FROM THE END OF THE QUADRUPOLES IN
      THE (N+1)TH.  DRIFT TUBE TO THE CENTRE OF THE
      (N+1)TH. GAP

      SA=(G(N+1)+(1.-FA)*LD(N+1))/(2.*V(N+1))
      X5=X4+(SA*XPRIM4)
      Y5=Y4+(SA*YPRIM4)
      R1=SQRT((ABS(X5))**2 +(ABS(Y5))**2 )
      CALL RESULT(N+1,XPRIM4,YPRIM4,X5,Y5,DX1,DY1)
      XPRIM5=XPRIM4+DX1
      YPRIM5=YPRIM4+DY1

      S31 IS THE TIME TAKEN BY THE PARTICLE TO TRAVERSE
      THE LENGTH FROM THE CENTRE OF THE (N+1)TH. GAP
      TO THE BEGINNING OF THE QUADRUPOLES IN THE
      (N+2)TH. DRIFT TUBE

      S31=(G(N+1)+(1.-FA)*LD(N+2))/(2.*V(N+2))
      X6=X5+S31*XPRIM5
      Y6=Y5+S31*YPRIM5

      TS2 IS THE TIME TAKEN BY THE PARTICLE TO TRAVERSE
      THE FIRST  HALF LENGTH OF THE QUADRUPOLES IN
      THE (N+2)TH. DRIFT TUBE

      TS2=(FA*LD(N+2))/(V(N+2)*2.)
      Q12=W*TS2
      Q22=COSH(Q12)
      Q32=SINH(Q12)
      Q42=COS(Q12)
      Q52=SIN(Q12)
      IF(W .EQ. 0.) GO TO 50
```

```
      Q62=Q52/W
      Q72=Q32/W
      GO TO 54

      THE FOLLOWING TWO STATEMENTS ARE USED FOR
      STRUCTURE WITHOUT QUADRUPOLES

   50 Q62=FA*LD(N+2)/(2.*V(N+2))
      Q72=Q62
   54 X(N+2)=(X6*Q42)+(XPRIM5*Q62)
      XPRIME(N+2)=-(X6*Q52*W)+(XPRIM5*Q42)
      XPRIM(N+2)=(ATAN(XPRIME(N+2)/V(N+2)))*57.29582
      Y(N+2)=(Y6*Q22)+(YPRIM5*Q72)
      YPRIME(N+2)=(Y6*Q32*W)+(YPRIM5*Q22)
      YPRIM(N+2)=(ATAN(YPRIME(N+2)/V(N+2)))*57.29582
      NA=N+1
      J2(N+1)=FLOAT(N+1)
      R(N+2)=SQRT((X(N+2)**2)+(Y(N+2)**2))
      IF((R(N+2)) .GT.  D ) GO TO 15
      IF((ABS(PHI(N+2))) .GT. 6.28318) GO TO 15
   89 CONTINUE

      OUTPUT IN TABULAR FORM

   15 WRITE(6,91)((K,X(K),Y(K),DPHI(K),DVEL(K),DENERG(K)),
     1K=1,NA)
   91 FORMAT((5X,I2,5(5X,E11.4)))

      OUTPUT IN GRAPHICAL FORM

      CALL PLOTNG (J2,NA,X,Y,L,M )
      CALL PLOT (0.0,0.0,999)
      STOP
      END
```

```
      THIS SUBROUTINE COMPUTES THE STRUCTURE DIMENSIONS

      SUBROUTINE STRUCT
      COMMON EM,VM1,F,R1,A,VM,L,FB,PH,DELTA1,LS(40),
     1G(40),ENERGS(40),ENERGY(40),DVEL(40),DPHI(40),
     1VS(40),LD(40),PHIS(40),PHI(40),ALPHA(40),V(40),
     1DENERG(40)
      DIMENSION LS1(40),PHIS1(40),V2(40),TT(40),R(40),
     1RPRIME(40)
      REAL LS1,LD,LS
      READ(5,42)PHS
   42 FORMAT(F6.1)
      R(1)=0.
      RPRIME(1)=0.
      VS(1)=SQRT(2.*EM*VM1)
      ENERGS (1)=.5*(VS(1)**2.)/EM
      TOTLEN=0.
      LS1(1)=(VS(1))/(2.*F)
      LD(1)=(LS1(1)/(1.+FB))
      PHIS(1)=(-90.+PHS)/57.29582
      PHIS(2)=PHS/57.29582
      DO 70 N=1,L
      G(N)=FB*LD(N)
      PHIS(N+1)=PHIS(2)
      S6=(.5*LD(N)*(1.+FB))/VS(N)
      R1=R(N)+S6*RPRIME(N)
      LD(N+1)=LD(N)
      LS1(N+1)=LS1(N)

      THE FOLLOWING ITERATION COMPUTES THE VALUES
      OF LD(N+1) AND LS1(N+1) CORRECT UPTO 7 DECIMAL
      PLACES

      DO 52 J=1,20
      LS(N)=(.5*(LD(N)+LD(N+1)))+G(N)
      D1=3.14159*R1/LS(N)
      D2=3.14159*A /LS(N)
      D3=(3.14159*G(N))/(2.*LS(N))
      D4=SIN(D3)/D3
      CALL BESI(D1,0,BI1,IERI)
      CALL BESI(D2,0,BI2,IER2)
      TT(N)=D4*BI1/BI2
      DELVS=(EM*VM*COS(PHIS(N+1))/VS(N))*TT(N)
      VS(N+1)=VS(N)+DELVS
      SS2=VS(N+1)/(2.*F)
      V1=SS2-LS1(N+1)
      IF (V1 .LT. 1. E-07) GO TO 53
      LS1(N+1)=SS2
      LD(N+1)=(SS2/(1.+.5*FB))-((FB*LD(N))/(2.+FB))
   52 CONTINUE
```

```
53   V2(N)=V1
     LS1(N+1)=SS2
     LD(N+1)=(SS2/(1.+.5*FB))-((FB*LD(N))/(2.+FB))
     LS(N)=(.5*(LD(N)+LD(N+1)))+G(N)
     TOTLEN=TOTLEN+LS(N)
     IF(R1 .EQ. 0.) GO TO 92
     CALL BESI(D1,1,BI3,IER3)
     C2=D4*BI3/BI2
     DELTA=(EM*VM*SIN(PHIS(N+1))/VS(N))*(C2/R1)
     GO TO 93
92   DELTA=0.
93   S4=.5*(LD(N+1)+G(N))/(VS(N+1))
     R(N+1)=R1+(S4*(-DELTA*R1+RPRIME(N)))
     RPRIME(N+1)=(-DELTA*R1)+RPRIME(N)
     DENGY=VM*((COS(PHIS(N+1))*TT(N))-(RPRIME(N)*
    1SIN(PHIS(N+1))*C2/VS(N)))
     ENERGS(N+1)=ENERGS(N)+DENGY
     PHIS1(N)=PHIS(N)*57.29582
  70 CONTINUE
     WRITE(6,30)((K,LD(K),G(K),TT(K),VS(K),ENERGS(K)),
    1K=1,L)
  30 FORMAT((5X,I2,5(5X,E11.4)))
     WRITE(6,78)TOTLEN
  78 FORMAT(/5X,E11.4)
     RETURN
     END
```

```
      THIS SUBROUTINE COMPUTES NONSYNCHRONOUS VELOCITY,
      PHASE,ENERGY AND THE CHANGE IN SLOPE OF THE
      TRAJECTORY IN THE GAP

      SUBROUTINE RESULT(N,XPRIM1,YPRIM1,XA,YA,DXPR,DYPR)
      COMMON EM,VM1,F,R1,A,VM,L,FB,PH,DELTA1,LS(40),
     1G(40),ENERGS(40),ENERGY(40),DVEL(40),DPHI(40),
     1VS(40),LD(40),PHIS(40),PHI(40),ALPHA(40),V(40),
     1DENERG(40)
      DIMENSION TT(40)
      REAL LS,LD
      ALPHA(N)=(VS(N)/V(N))-1.
      IF (N .GT. 1) GO TO 81
      PHI(2)=((PH)/57.29582)+((90./57.29582)*ALPHA(1))
      GO TO 82
   81 PHI(N+1)=PHI(N)+3.14159*ALPHA(N)
   82 DPHI(N+1)=(PHI(N+1)-PHIS(N+1))*57.29582
      D1=3.14159*R1/LS(N)
      D2=3.14159*A /LS(N)
      D3=(3.14159*G(N))/(2.*LS(N))
      D4=SIN(D3)/D3
      CALL BESI(D1,0,BI1,IERI)
      CALL BESI(D2,0,BI2,IER2)
      CALL BESI(D1,1,BI3,IER3)
      CALL BESI(D1,2,BI4,IER4)
      CALL BESI(D2,1,BI5,IER5)
      D5=((((.7853975/LS(N))*(G(N)**2.)*COS(D3))
     1-(.5*G(N)*SIN(D3)))/(D3**2.))
      TT(N)=D4*BI1/BI2
      C2=D4*BI3/BI2
      C3=-(3.14159/(LS(N)**2.))*(((D4*(R1*BI2*BI3
     1-A*BI1*BI5))/(BI2**2.))+((BI1/BI2)*D5))
      C4=-(3.14159/(LS(N)**2.))*((D4*((((BI2*LS(N)
     1/3.14159)*(BI3+D1*BI4))-A*BI3*BI5)/(BI2**2.
     1)))+((BI3/BI2)*D5))
      A3=TT(N)+ALPHA(N)*LS(N)*C3
      A5=C2-ALPHA(N)*LS(N)*C4
      DELV=(EM*VM*COS(PHI(N+1))/V(N))*A3
      V(N+1)=V(N)+DELV
      DVEL(N)=V(N)-VS(N)
      IF(R1 .LT. 1.E-07) GO TO 14
      DELTA1=(EM*VM*SIN(PHI(N+1))/V(N))*(A5/R1)

      COMPUTATION OF THE CHANGE IN TRANSVERSE VELOCITIES
      IN THE VERTICAL AND THE HORIZONTAL PLANES
      DENOTED BY DXPR AND DYPR RESPECTIVELY

   91 IF(((ABS(XA)) .GT. 1.E-07) .AND.((ABS(YA))
     1.GT. 1.E-07)) GO TO 11
      IF(((ABS(XA)) .GT. 1.E-07) .AND.((ABS(YA))
```

[illegible]

[illegible]

[illegible]

[illegible]

[illegible]

[illegible]

[illegible]

[illegible]

```
  1.LT. 1.E-07)) GO TO 12
   GO TO 13
11 ANGL=ATAN((ABS(YA))/ (ABS(XA)))
   GO TO 15
12 DXPR=-(DELTA1*R1)
   DYPR=0.0
   GO TO 7
13 DXPR=0.
   DYPR=-(DELTA1*R1)
   GO TO 7
15 DXPR=-(DELTA1*R1*COS(ANGL))
   DYPR=-(DELTA1*R1*SIN(ANGL))
7  IF(XA .LT. 0.0) GO TO 16
   GO TO 17
16 DXPR=-DXPR
17 IF(YA .LT. 0.0) GO TO 18
   GO TO 19
18 DYPR=-DYPR
   GO TO 19
14 DELTA1=0.
   DXPR=0.
   DYPR=0.
   RPRIM6=SQRT((XPRIM1**2)+(YPRIM1**2))
   GO TO 20
19 XPRIM6=XPRIM1+DXPR/2.
   YPRIM6=YPRIM1+DYPR/2.
   RPRIM6=((XA*XPRIM6)/R1)+((YA*YPRIM6)/R1)
20 DENG=VM*((COS(PHI(N+1))*A3)-((RPRIM6/V(N))*
  1SIN(PHI(N+1))*A5))
   ENERGY(N+1)=ENERGY(N)+DENG
   DENERG(N)=ENERGY(N)-ENERGS(N)
   RETURN
   END
```

```
 THIS SUBROUTINE PLOTS GRAPHS FOR TRANSVERSE
 EXCURSIONS IN THE VERTICAL AND THE HORIZONTAL
 PLANES.

 SUBROUTINE PLOTNG(J2,NA,X,Y,L,M)
 DIMENSION J2(40),X(40),Y(40)
 REAL J2
 DC=5.
 CD=4.
 CDC=CD+1.

 J2 IS THE ABSCISSA ARRAY NAME DENOTING THE
 MIDDLE OF EACH DRIFT TUBE AND X,Y ARE THE
 ORDINATE ARRAY NAMES DENOTING EXCURSIONS IN
 THE VERTICAL AND THE HORIZONTAL PLANES
 RESPECTIVELY

 SET UP SCALE FOR X ,Y AND J2

 J2(NA+1)=1.
 J2(NA+2)=(FLOAT(L))/DC
 SC1=-.03
 SC2=.06
 X(NA+1)=SC1
 X(NA+2)=(SC2/CD)
 Y(NA+1)=SC1
 Y(NA+2)=(SC2/CD)

 DRAW THE AXES FOR THE VERTICAL EXCURSIONS

 CALL AXIS(0.0,0.0,' ',-1,DC,0.0,J2(NA+1),
1J2(NA+2),20.0)
 CALL AXIS(0.0,0.0,' ',1,CD,90.0,X(NA+1),
1X(NA+2),20.0)

 DRAW THE TRAJECTORY FOR VERTICAL EXCURSIONS

 CALL LINE(J2,X,NA,1,1,M)

 THIS SETS THE ORIGIN FOR THE NEXT GRAPH

 CALL PLOT(0.0,CDC,-3)

 DRAW THE AXES FOR HORIZONTAL EXCURSIONS

 CALL AXIS(0.0,0.0,' ',-1,DC,0.0,J2(NA+1),
1J2(NA+2),20.0)
 CALL AXIS(0.0,0.0,' ',1,CD,90.0,Y(NA+1),
1Y(NA+2),20.0)

 DRAW THE TRAJECTORY FOR HORIZONTAL EXCURSIONS

 CALL LINE(J2,Y,NA,1,1,M)
 CALL PLOT(0.0,-CDC,-3)
 RETURN
 END
```

4.3 Computer Output and Discussion of Results

4.3.1 Structure Dimensions and the Synchronous Parameters

The accelerator structure dimensions, transit time factor, velocity and the energy of the synchronous particle for each section have been computed for the following nominal input specifications. The result is listed in table 1.

Input specifications:

Inner radius of the drift tube = 4 cm
Peak operating voltage in the gap = 150 Kv
Voltage of the particle at injection = 300 Kv
Operating frequency of the structure = 30 KHz
Charge to mass ratio of the particle = 30 coulombs/Kg
Synchronous phase at the gap centre = -30°
Ratio of the gap length to the drift tube length = .25
The synchronous particle travels along the axis of the accelerator.

4.3.2 Particle Trajectories

Fig. 4.2 shows the trajectories of two nonsynchronous

Table 1

Structure Dimensions and Synchronous Parameters

N	Length of Nth. drift tube (cm)	Length of Nth. gap (cm)	Transit time factor	Synchronous velocity (Km/Sec)	Synchronous energy (Mv)
1	5.657	1.414	.5317	4.243	.3
2	6.380	1.595	.5929	4.731	.3691
3	7.024	1.756	.6407	5.219	.4461
4	7.661	1.915	.6806	5.698	.5293
5	8.280	2.070	.7136	6.163	.6177
6	8.879	2.220	.7411	6.615	.7104
7	9.460	2.365	.7642	7.051	.8067
8	10.020	2.505	.7837	7.474	.9060
9	10.560	2.641	.8004	7.882	1.0080
10	11.090	2.772	.8147	8.278	1.1120
11	11.600	2.900	.8271	8.662	1.2180
12	12.090	3.024	.8379	9.034	1.3250
13	12.570	3.144	.8474	9.395	1.4340
14	13.040	3.261	.8559	9.747	1.5440
15	13.500	3.374	.8634	10.090	1.6550
16	13.940	3.485	.8701	10.420	1.7670
17	14.370	3.593	.8762	10.750	1.8800
18	14.800	3.699	.8816	11.070	1.9940
19	15.210	3.802	.8866	11.380	2.1090
20	15.610	3.903	.8911	11.680	2.2240
21	16.010	4.002	.8953	11.940	2.3400
22	16.400	4.099	.8991	12.270	2.4560
23	16.780	4.190	.9025	12.550	2.5730
24	17.150	4.287	.9058	12.830	2.6900
25	17.520	4.379	.9088	13.110	2.8080
26	17.870	4.469	.9115	13.380	2.9260
27	18.230	4.557	.9141	13.640	3.0440
28	18.580	4.644	.9165	13.910	3.1630
29	18.920	4.729	.9188	14.160	3.2820
30	19.250	4.814	.9209	14.420	3.4010

Total length of the structure = 5.05 Meters

Note: Input specification for the design of the structure is given in section 4.3.1.

particles, with same charge to mass ratio and injection voltage as the synchronous particle, in the drift tube structure designed above. The particles are injected at the middle of the first drift tube. One particle is injected on the axis with a slope such that the projections of the initial trajectory on the horizontal and the vertical planes make angles of 0.2 degrees with the axis of the accelerator. The other particle is injected paraxially with an initial horizontal and vertical displacement of .2 cm each. It is seen that, in the structure without quadrupoles, the particle injected on the axis collides with the 18th drift tube wall and the particle injected paxaxially collides with the 14th drift tube wall. On the other hand, if quadrupoles are used both the particles traverse the complete structure of 30 drift tubes without being intercepted.

It can also be seen from fig. 4.2 that the trajectories of the particle for a structure with quadrupoles have small oscillations with a period of two section length. The amplitudes of these oscillations increase with the increase in transverse excursion of the particle. The reason for this behaviour is that the individual quadrupole action is much stronger than the overall focusing effect and that as the excursions increase the focusing and the defocusing forces become more intense

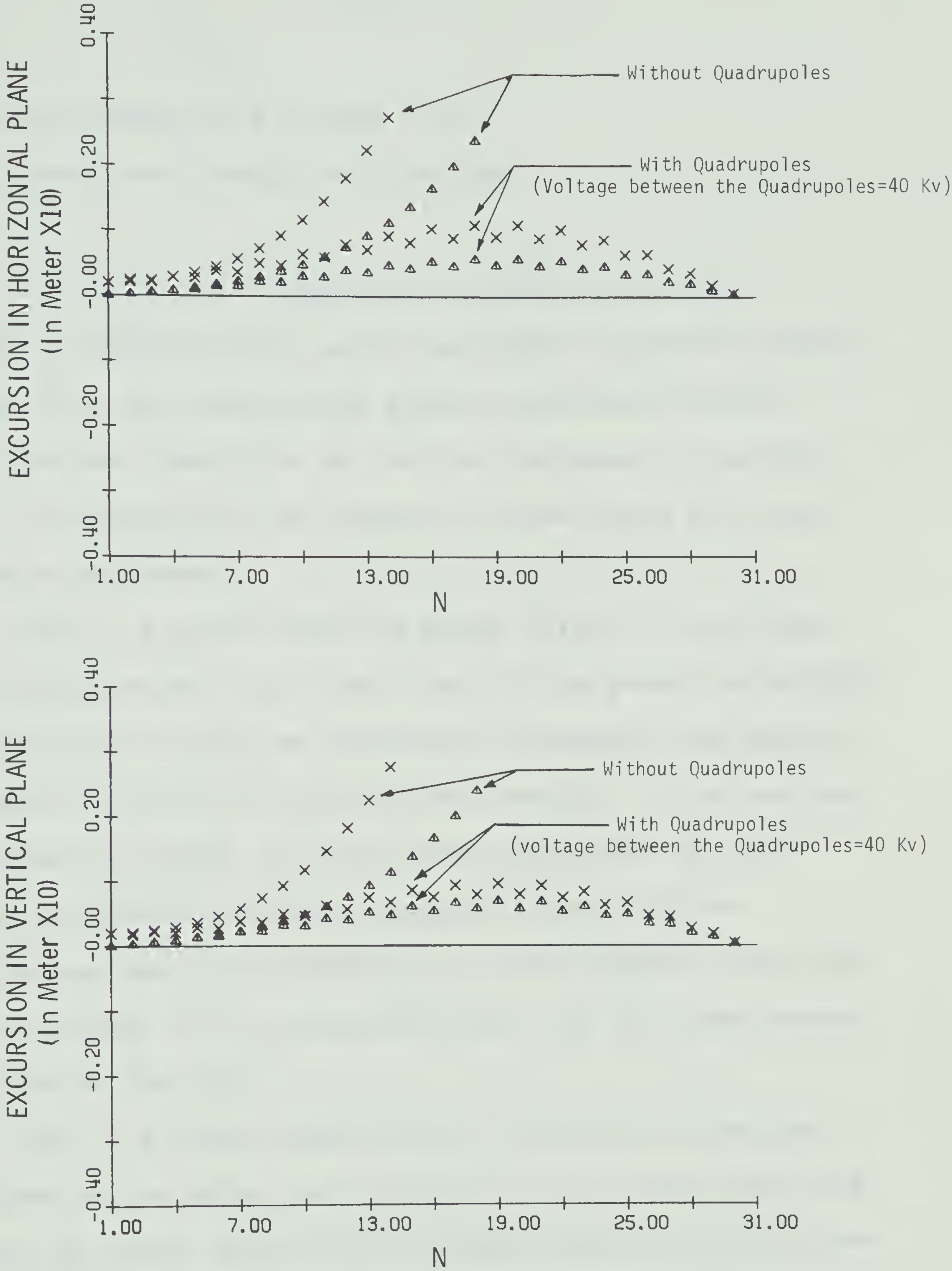

Note: N is the middle of the Nth. drift tube.
The projections of the slope of the trajectory △ at injection in both horizontal and vertical planes are .2 degree each. The particle for trajectory × is injected paraxially. All other injection conditions are synchronous.

FIG.4.2 Transverse Excursions With and Without Quadrupoles

(refer to equations 2-26 and 2-27)

4.3.3 Phase and Energy Oscillations

In fig. 4.3 the phase oscillations and the energy oscillations for particles whose injection phases differ from the synchronous phase have been plotted. The structure used here is the one designed in section 4.3.1. The particle is assumed to move along the axis of the accelerator.

Fig. 4.3 shows that the phase slips in one direction or the other i.e., the slope of the phase trajectory is positive or negative depending on whether the energy is above or below the synchronous energy. It is noticed that when the phase is synchronous the slope of the energy (difference between nonsynchronous and the synchronous energy) trajectory is zero implying that the gain in energy of the nonsynchronous and the synchronous particle is the same.

Fig. 4.4 shows the effect of different injection energies on the phase oscillations. It is seen that the damping of phase oscillation becomes slower as the injection energy increases above the synchronous injection energy. This is because the velocity change for a given change in energy decreases as the particle energy increases. Hence $\Delta\phi_n$ and thus the rate of phase damping decreases as the energy increases.

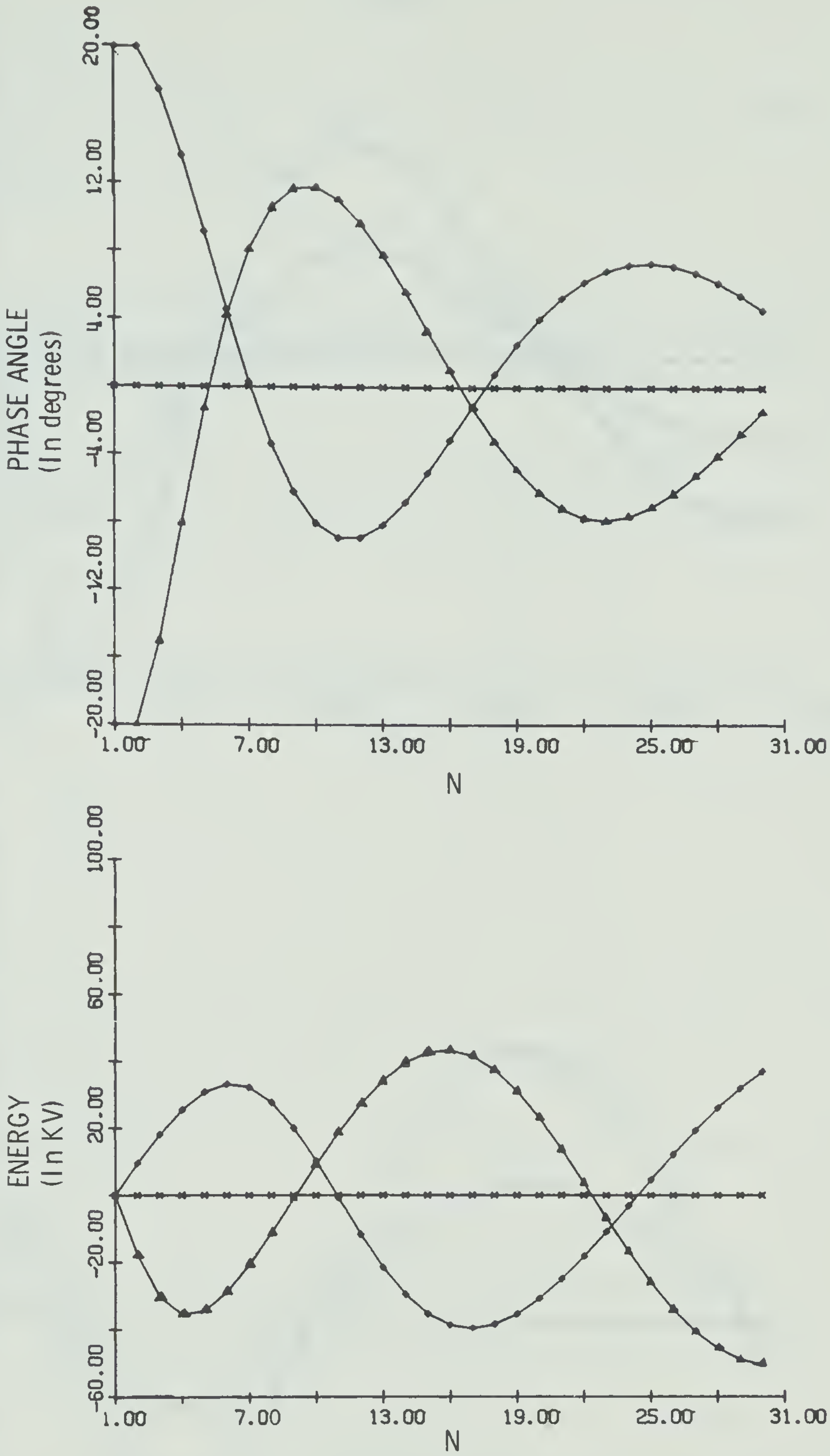

Note: N is the middle of the Nth. drift tube. The ordinate above or below the horizontal lines through the zero phase and zero energy indicates that the nonsynchronous phase and energy are greater than the synchronous phase and energy by that amount. The injection parameters, except for the injection phase, of the particles are the same as those of the synchronous particle. Trajectories with the same symbol in phase and energy plots correspond to the same set of injection conditions.

FIG. 4.3 Phase and Energy Oscillations for Different Injection Phases and Same Injection Energy.

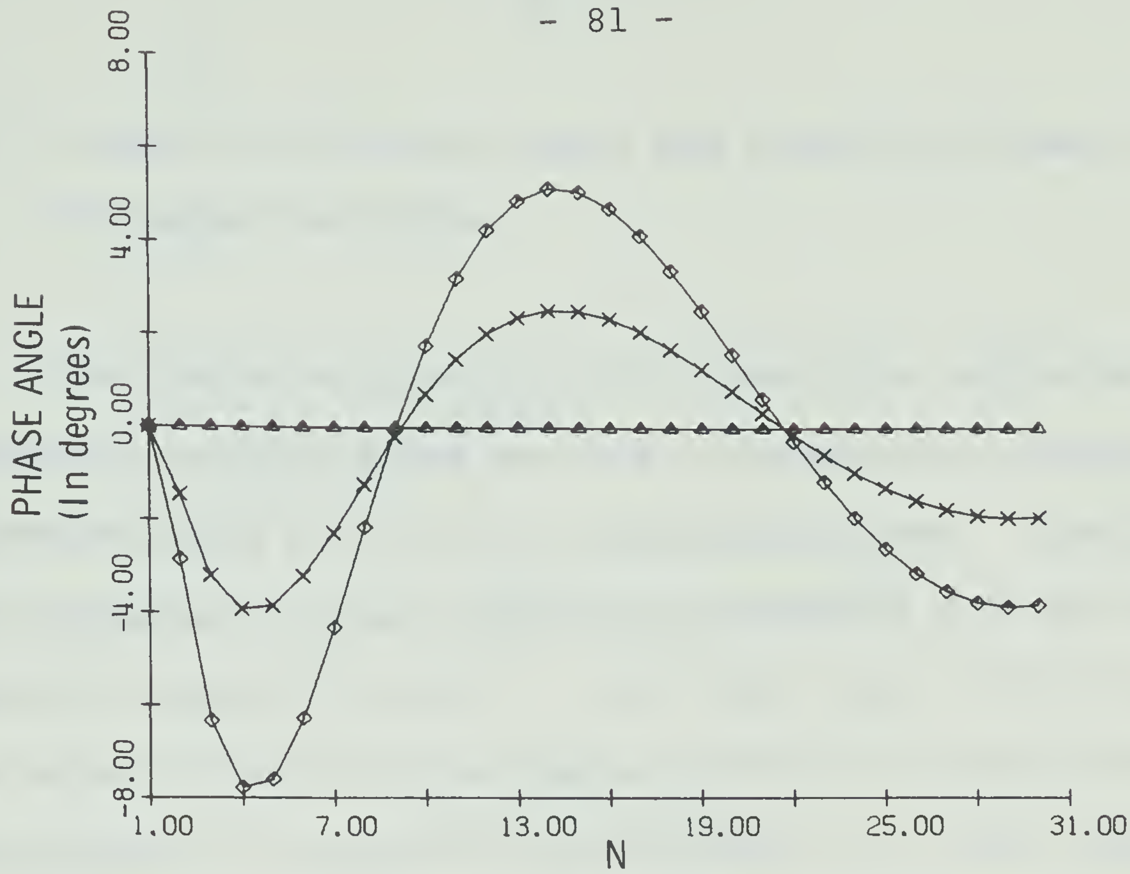

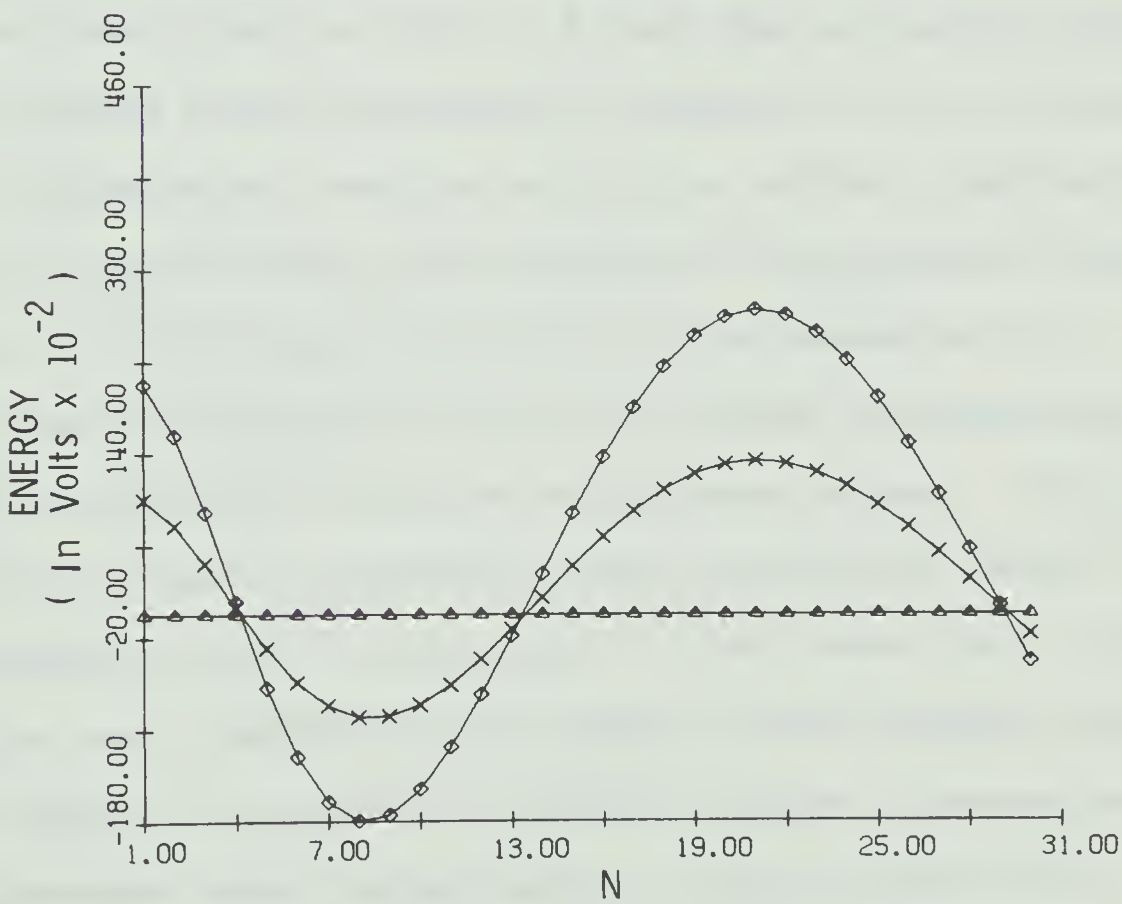

Note: The injection parameters, except for the injection energy, are the same as those of the synchronous particle.

FIG. 4.4 Phase and Energy Oscillations for Different Injection Energies and Same Injection Phase.

4.3.4 Range of Injection Angle and Injection Phase for Accepted Particles

The shaded area of fig. 4.5 shows the region of accepted injection phase and the corresponding accepted injection angle at (0°-90°) synchronous phase. Similarly the boundaries of the acceptance parameters for the synchronous phases (-15°-90°), (-30°-90°) and (-45°-90°) are also shown (note that the factor -90° is included because the particle is injected at the middle of a drift tube). It is clear from the fig. 4.5 that the allowable injection angles have been greatly improved for the structure with quadrupoles over the structure without quadrupoles. It is also seen that the decrease of synchronous phases from (-0°-90°) up to (-45°-90°) is accompanied by a decrease in acceptable injection angles corresponding to these particular injection synchronous phases. This result is due to increased radial defocusing forces (refer to equation 2-8) in the gaps. On the other hand, if particles are injected with an angle of zero degree, then the range of acceptable injection phases increases as the synchronous phase is decreased. This is due to the increased axial focusing forces (given by equation 2-23) and due to the absence of a radial defocusing force.

It may also be noticed that the acceptable injection angle gradually increases to a peak value as the injection phase is increased from the injection synchronous

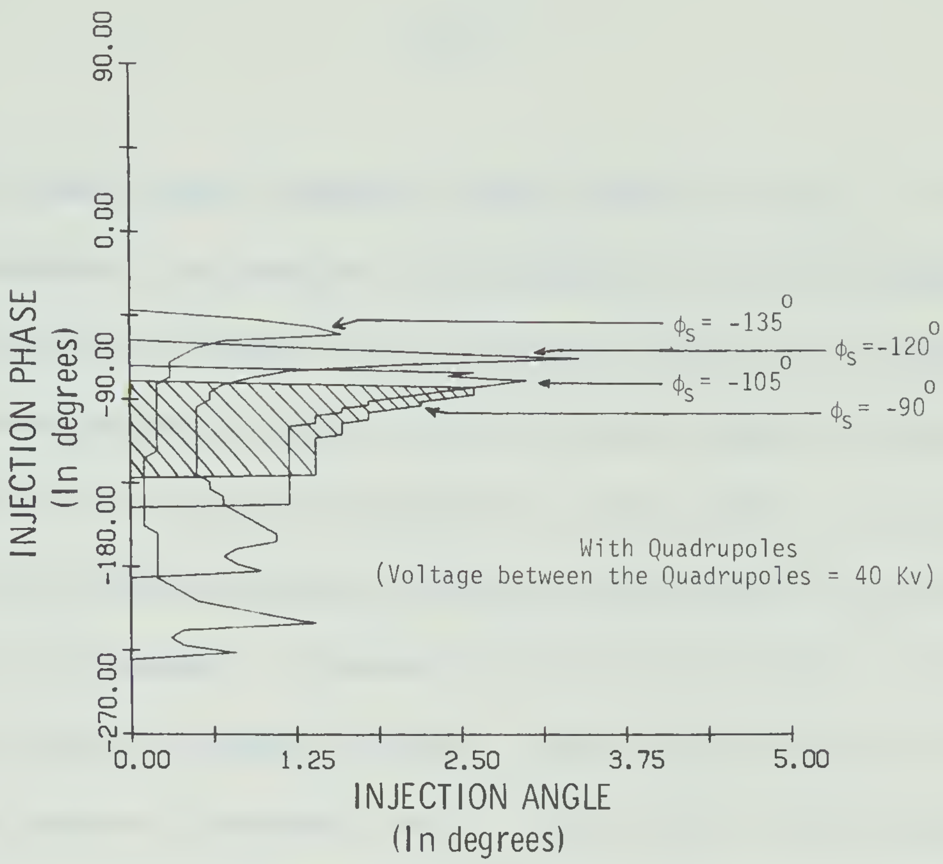

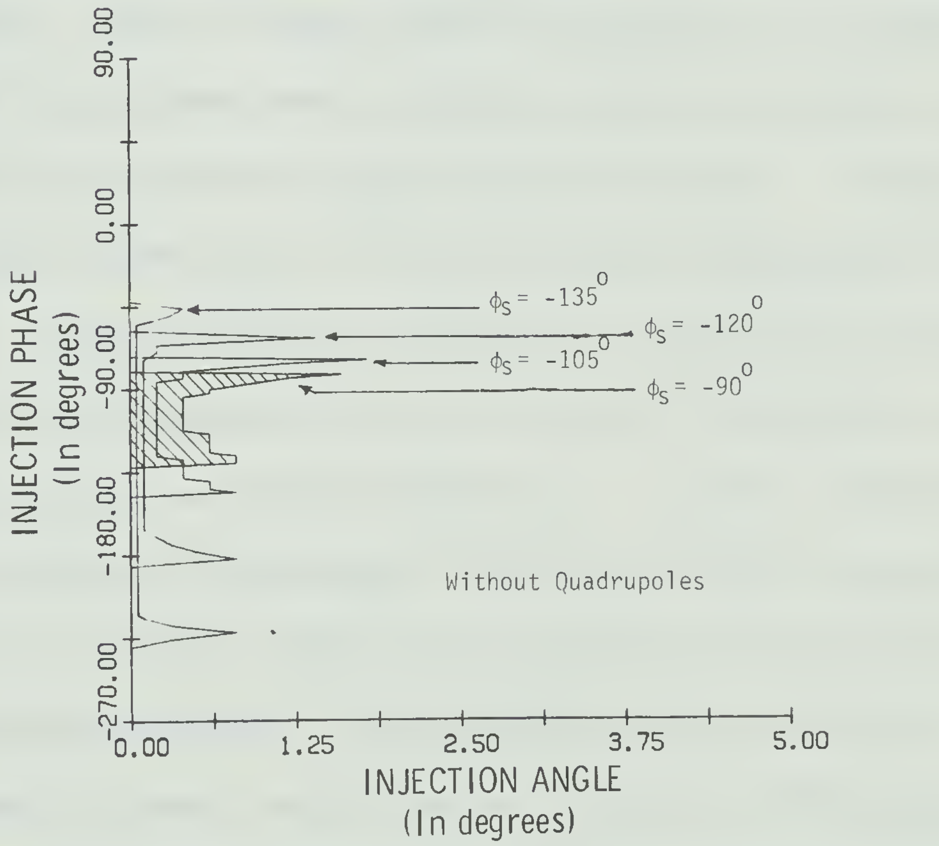

Note: The particle is injected on the axis of the accelerator. ϕ_s is the synchronous phase at the injection point i.e. at the middle of the first drift tube. The injection angle is the angle of the trajectory of the particle at the point of injection projected in the horizontal and the vertical planes.

FIG. 4.5 The Range of Injection Phase and Injection Angle at the Axis for Accepted Microparticles.

phase and then very rapidly drops down to zero. This occurs because the radial defocusing force decreases as the injection phase is increased from the injection synchronous phase. When the injection phase crosses the (-0°-90°) injection phase the net radial focusing force in the gap becomes positive and hence the angle of injection increases. However at the same time the axial focusing effect becomes weaker, and eventually as the injection phase crosses (-90°), the axial field becomes defocusing. Thus if the injection phase is further increased the phase very quickly slips by greater than 360° and the injection angle falls to zero. It may also be seen from fig. 4.5 that as one decreases the injection phase below the injection synchronous phase the radial defocusing force at the gap increases and thus the injection angle decreases. As the injection phase is further decreased, the axial force causes the particle to execute larger and larger oscillations about the synchronous phase. Consequently the particle alternates in phase such that the radial defocusing force is alternately very much stronger and then very much weaker than the radial defocusing force at the synchronous phase. It is believed that the net effect of this large amplitude of oscillations leads to an increased acceptance of injection angles. However if the

injection phase is further decreased the initial defocusing forces become so large that the particle will immediately strike the structure wall and thus the injection angle falls to zero.

4.3.5 Effect of Variable Charge to Mass Ratio on Particle Trajectories for the Structure Designed in Sec. 4.3.1

It is seen from fig. 4.6 that in the structure without quadrupoles the particle experiences more and more defocusing force as the charge to mass ratio increases beyond the design value of 30 coulombs/Kg. This may also be seen from equation 2-8 which shows that the defocusing force in the gaps increases with an increase in charge to mass ratio.

From fig. 4.7 it is seen that in the structure with quadrupoles the overall focusing force in the first few sections diminishes with increase in charge to mass ratio. But after these first few sections the overall focusing force increases rapidly with increase in charge to mass ratio. This is due to the fact that increase in charge to mass ratio increases the focusing force of the quadrupoles (refer to equation 2-28, 2-29). In the first few sections the increase in defocusing force in the gap is larger than the increase in focusing force of the

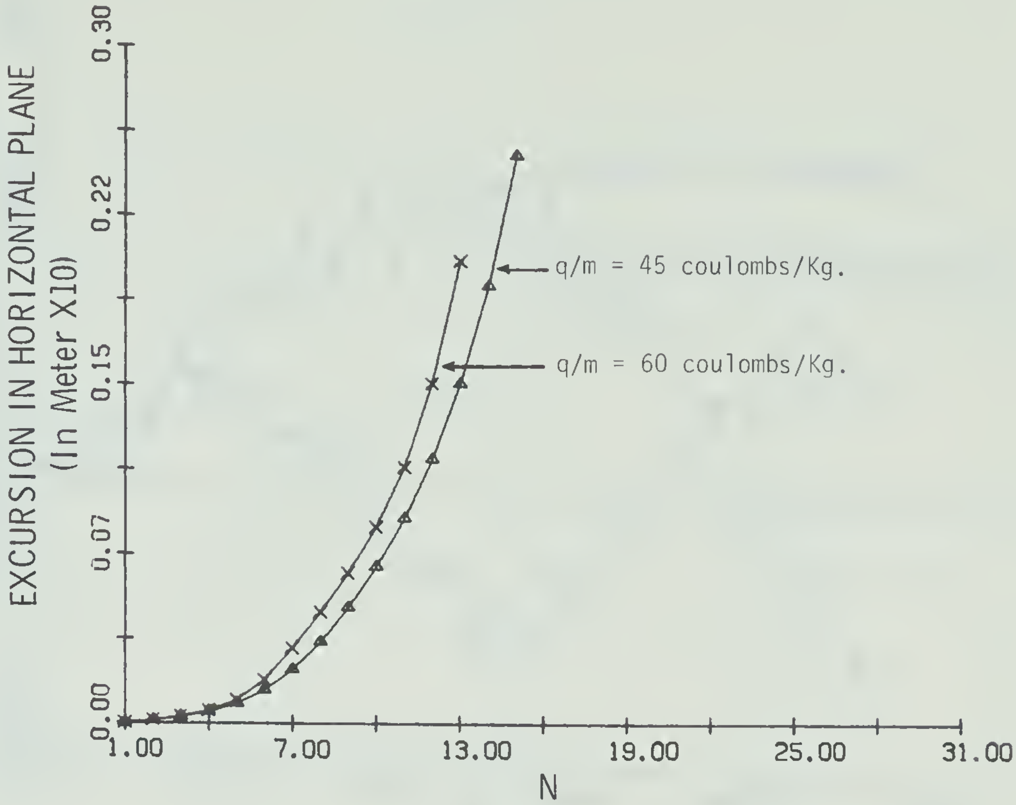

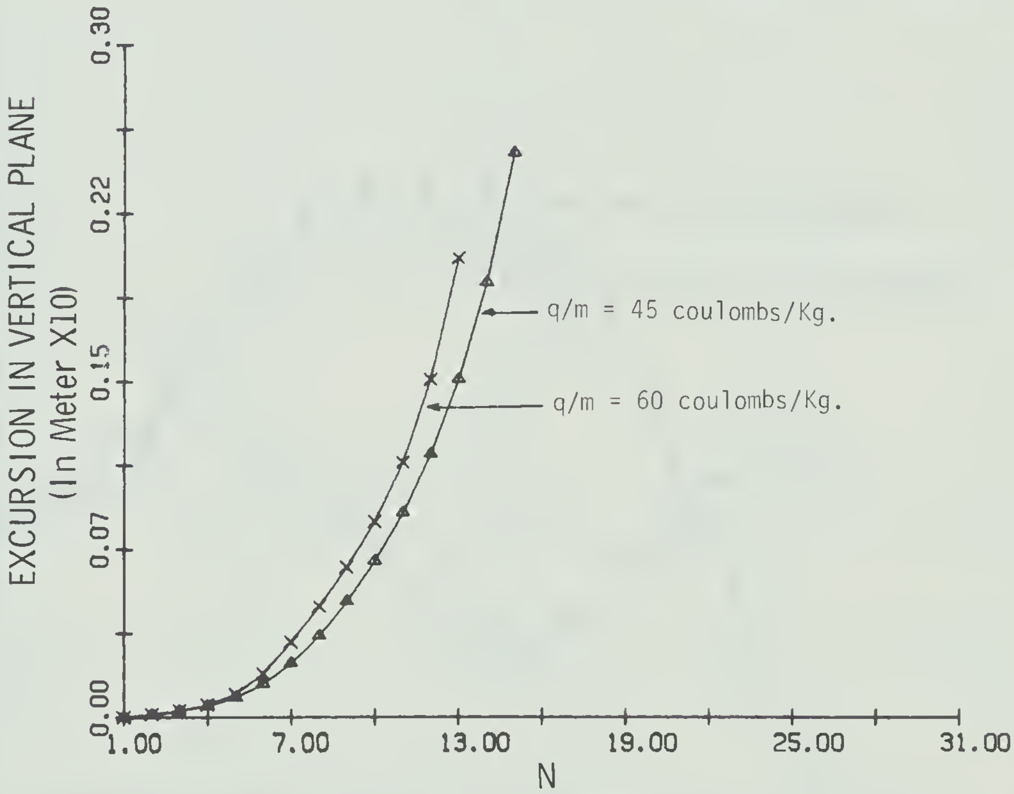

Note: The particle is injected on the axis at an angle of .1 degree in the horizontal and the vertical planes. The injection phase is synchronous.

FIG. 4.6 Transverse Excursions of Particles With Different Charge to Mass Rations for Structure Without Quadrupoles Nominally Designed for $\frac{q}{m}$ = 30 coulombs/Kg.

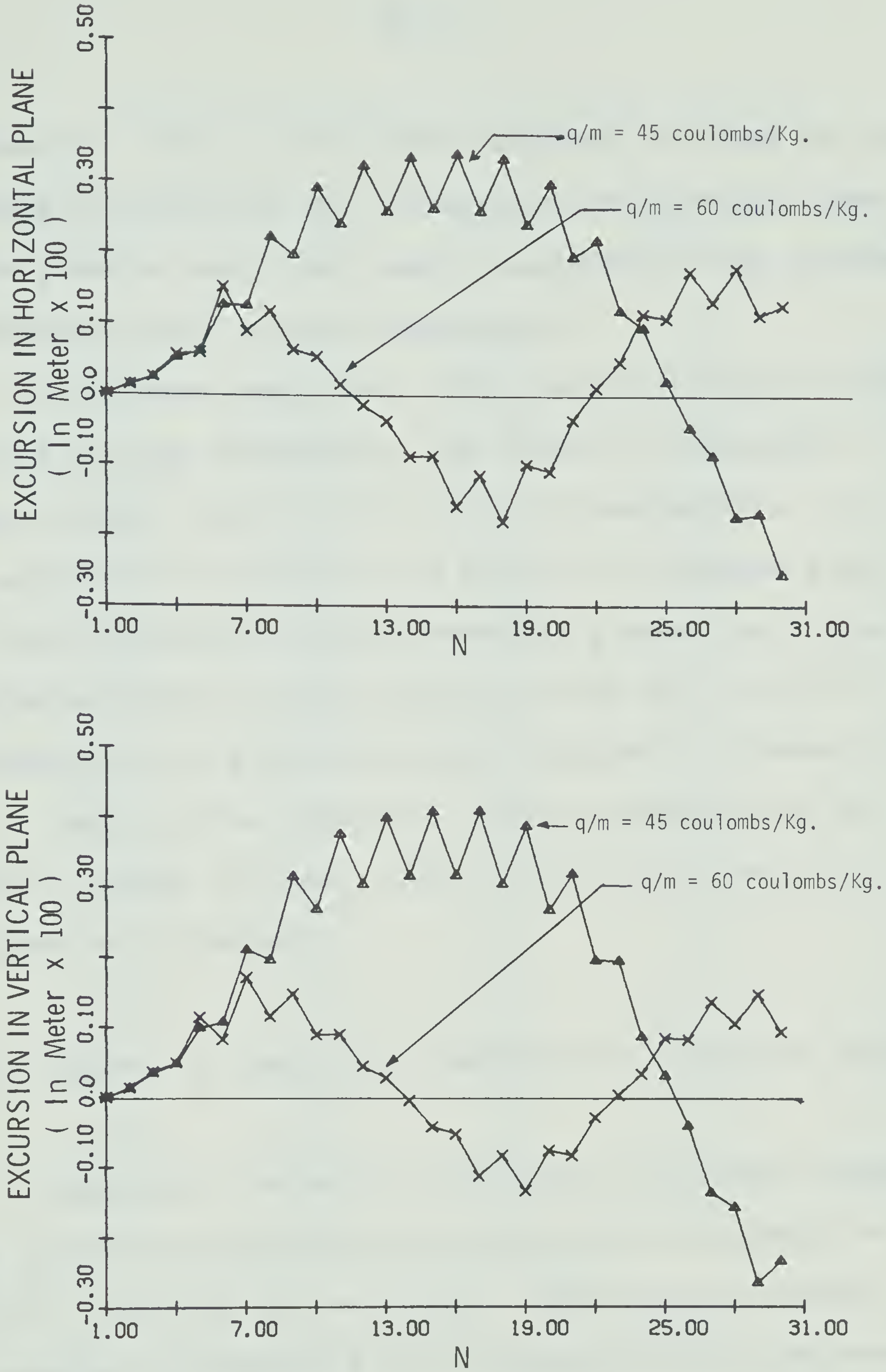

Note: Same note as in Fig. 4.6

FIG. 4.7 Transverse Excursions of Particles With Different Charge to Mass Ratios for Structure with Quadrupoles Nominally Designed for

$$\frac{q}{m} = 30 \text{ coulombs/Kg.}$$

quadrupoles. But at the later sections, because of the increase in velocity, the increase in defocusing force in the gaps is very, very small compared to the increase in focusing force of the quadrupoles.

It has been seen that for a particle moving along the axis of the accelerator the range of acceptable charge to mass ratio is 26.2 to 83.5 coulombs/Kg. If the particle is injected at a slope of .2 degree each with the horizontal and the vertical planes the range of acceptable charge to mass ratio is also 26.2 to 83.5 coulombs/Kg in a structure with quadrupole voltage of 40 Kv. But for the structure without quadrupoles the range of charge to mass ratio is zero for a particle injected at .2 degree.

4.3.6 Effect of operating Frequency on Structure Design

Additional tables of accelerator structure dimensions have been computed for an operating frequency of 50 KHz. The rest of the nominal input specifications are same as in section 4.3.1, except that for one case the drift tube radius has been halved from 4 cm. to 2 cm. The dimensions and the other synchronous parameters are listed in table 2 and table 3.

It is seen that at 50 KHz the total length of the

Table 2

Structure Dimensions and Synchronous Parameters

N	Length of Nth. drift tube (cm)	Length of Nth. gap (cm)	Transit time factor	Synchronous velocity (Km/Sec)	Synchronous energy (Mv)
1	3.394	.8485	.2184	4.243	.3
2	3.572	.8931	.2441	4.443	.3284
3	3.743	.9357	22696	4.657	.3601
4	3.925	.9811	.2962	4.883	.3951
5	4.115	1.0290	.3135	5.119	.4336
6	4.312	1.0780	.3510	5.366	.4756
7	4.517	1.1290	.3785	5.621	.5212
8	4.727	1.1820	.4056	5.883	.5704
9	4.943	1.2360	.4322	6.152	.6231
10	5.162	1.2910	.4580	6.426	.6792
11	5.385	1.3460	.4829	6.703	.7387
12	5.610	1.4020	.5066	6.984	.8014
13	5.836	1.4590	.5293	7.267	.8673
14	6.063	1.5160	.5507	7.551	.9360
15	6.291	1.5730	.5710	7.835	1.0080
16	6.518	1.6290	.5900	8.119	1.0820
17	6.744	1.6860	.6080	8.402	1.1580
18	6.970	1.7420	.6248	8.684	1.2370
19	7.194	1.7980	.6406	8.964	1.3190
20	7.417	1.8540	.6554	9.243	1.4020
21	7.637	1.9090	.6692	9.519	1.4870
22	7.856	1.9640	.6822	9.793	1.5740
23	8.073	2.0180	.6944	10.060	1.6620
24	8.288	2.0720	.7058	10.330	1.7530
25	8.501	2.1250	.7165	10.600	1.8440
26	8.712	2.1780	.7265	10.860	1.9370
27	8.920	2.2300	.7360	11.120	2.0320
28	9.126	2.2810	.7448	11.380	2.1270
29	9.330	2.3320	.7532	11.640	2.2240
30	9.531	2.3830	.7611	11.890	2.3220

Total length of the structure = 2.437 Meters.

Note: Operating frequency of the structure = 50 KHz
Other input specifications are same as in section 4.3.1.

Table 3

Structure Dimensions and Synchronous Parameters

N	Length of Nth. drift tube (cm)	Length of Nth. gap (cm)	Transit time factor	Synchronous velocity (Km/Sec)	Synchronous energy (Mv)
1	3.394	.8485	.6360	4.243	.3
2	3.913	.9784	.6963	4.827	.3826
3	4.355	1.0890	.7388	5.389	.4731
4	4.781	1.1950	.7719	5.923	.5690
5	5.185	1.2960	.7978	6.431	.6693
6	5.570	1.3930	.8185	6.915	.7729
7	5.937	1.4840	.8353	7.376	.8793
8	6.289	1.5720	.8493	7.817	.9878
9	6.626	1.6570	.8609	8.241	1.0980
10	6.951	1.7380	.8708	8.648	1.2100
11	7.263	1.8160	.8793	9.040	1.3230
12	7.566	1.8910	.8867	9.419	1.4370
13	7.858	1.9650	.8931	9.786	1.5520
14	8.142	2.0350	.8987	10.140	1.6680
15	8.417	2.1040	.9038	10.490	1.7850
16	8.685	2.1710	.9082	10.820	1.9030
17	8.946	2.2370	.9122	11.150	2.0210
18	9.200	2.3000	.9159	11.470	2.1390
19	9.449	2.3620	.9191	11.780	2.2580
20	9.691	2.4230	.9221	12.080	2.3770
21	9.929	2.4820	.9248	12.380	2.4970
22	10.160	2.5400	.9273	12.670	2.6170
23	10.390	2.5970	.9297	12.960	2.7380
24	10.610	2.6530	.9318	13.240	2.8590
25	10.830	2.7080	.9337	13.510	2.9800
26	11.050	2.7620	.9356	13.780	3.1010
27	11.260	2.8140	.9373	14.050	3.2230
28	11.470	2.8660	.9389	14.310	3.3440
29	11.670	2.9170	.9403	14.560	3.4660
30	11.870	2.9680	.9417	14.810	3.5880

Total length of the structure = 3.137 Meters.

Note: Inner radius of the drift tubes = 2 cm
Operating frequency of the structure = 50 KHz
Other input specifications are same as in section 4.3.1

structure for 30 sections is almost half of that of the structure designed for 30 KHz. It is important to notice that for 30 sections the energy gain for the structure designed at 30 KHz is much larger than that for the structure designed for 50 KHz, in the case where the drift tube radius has been held constant. The reason for this behavious is that the ratio a/LS_n increases and hence the transit time factor decreases, as may be seen from equation A1-10 of Appendix 1. On the other hand it may also be seen from Table 3 that if the drift tube radius for the 50 KHz structure is halved, then the transit time factor, and hence the overall energy gain is greatly increased over than shown in Table 2.

From fig. 4.8 it is seen that the particle injected on the axis of the 50 KHz structure at a given slope collides with the 24th drift tube wall of the structure, if there are no quadrupoles. If the particle is injected at the same slope into the structure with quadrupoles (voltage between quadrupoles is 40 Kv) it strikes the quadrupole surface of the 21st drift tube. The reason is that although the transverse excursions of the particle are less in the structure with quadrupoles, the maximum permissible transverse excursion is decreased because of the reduced aperture. Thus the net gain in introducing the quadrupoles at 40 Kv is negative. However, the gain

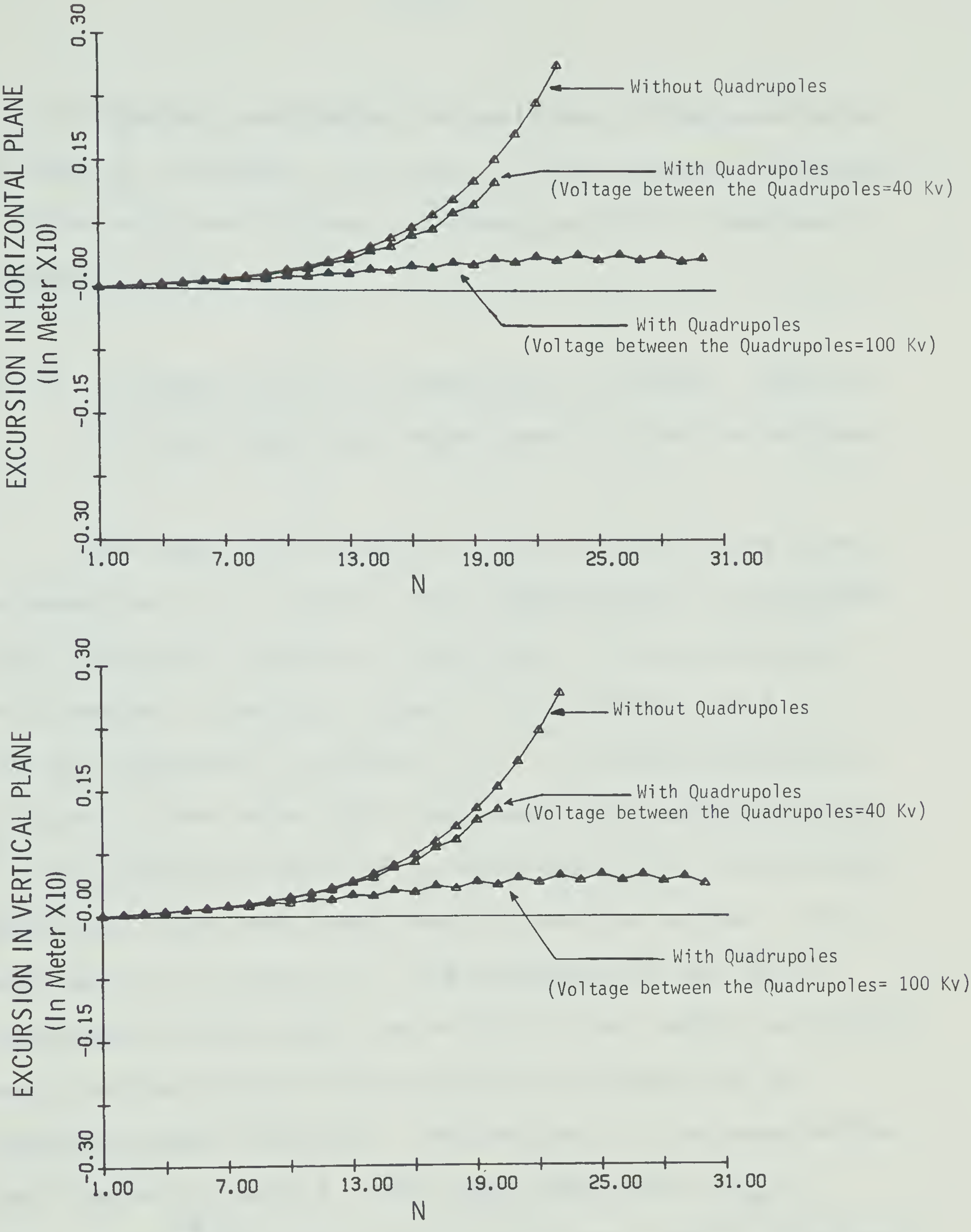

Note: The injection conditions of the particle are the same as for the trajectory ▲ of Fig. 4.2.

FIG. 4.8 Transverse Excursions for Structure With and Without Quadrupoles Designed at 50 KHz

in introducing quadrupoles is positive if the quadrupole voltage is increased. In fig. 4.8 the particle traverses all the sections without interception with a quadrupole voltage of 100 Kv.

4.3.7 A Comparison of the Equations of Motion Derived in This Thesis and Those used by Previous Workers

The numerical values of $-\Delta\dot{r}_n$, $\Delta\dot{z}_n$ and $\Delta E_n/q$ given by equation 2-8, 2-20 and 2-22 respectively are computed for a particle injected on the axis of the accelerator at a certain injection slope. The structure used is the one designed in section 4.3.1. The above equations are new in the sense that they are better approximations to the particle motion in an accelerator gap, than those equations that have been used by previous workers (references 6, 7, 8 and 14). The advantage of the above equations is that they are valid for any radial excursion and that the transit time factor is correct for any nonsynchronous velocity. The results of the computation are listed in table 4. The same quantities $-\Delta\dot{r}_{nold}$, $\Delta\dot{z}_{nold}$ and $\frac{\Delta E_{nold}}{q}$ given by the equations, used by previous authors, as shown below are computed for the same set of injection conditions and the same structure as above.

$$-\ \Delta\dot{r}_{nold} = (q/m)(\Pi/LSn)(Sin\phi_n/v_n)(V_m)(T_{s,n}(r))\text{-------}(4\text{-}1)$$

$$\Delta\dot{Z}_{nold} = (q/m)(COS\phi_n/v_n)(V_m)(T_{s,n}(r))\text{---------------}(4\text{-}2)$$

$$\Delta E_{nold}/q = (COS\phi_n)(V_m)(T_{s,n}(r))\text{---------------------}(4\text{-}3)$$

The results of the above computation are given in table 5

Upon comparing table 4 and table 5 it is found that the results of the computation by the two different sets of formulas agree very well for the first few sections. However, in later sections, when the particle no longer travels near the axis and its velocity is no longer synchronous, the difference between the two sets of formulas becomes important. This is evident from the results given in the two tables. The parameters have been computed up to the 24th section because the particle is intercepted by the 25th drift tube wall.

Table 4

Numerical Values of the Excursions, and $\Delta\dot{r}_n$, $\Delta\dot{Z}_n$ and $\Delta E_n/q$ Given by the Equations 2-8, 2-20 and 2-22

N	$\Delta\dot{r}_n$ (Meter/sec)	$\Delta\dot{Z}_n$ (Km/sec)	$\Delta E_n/q$ (Mv)	X(N) (cm)	Y(N) (cm)
1	-.416	.4884	.06907	.0	.0
2	-1.155	.4884	.07702	.01006	.01006
3	-1.823	.4784	.08324	.02111	.02111
4	-2.470	.4656	.08842	.03390	.03390
5	-3.135	.4513	.09272	.04923	.04923
6	-3.844	.4367	.09630	.06785	.06785
7	-4.619	.4225	.09930	.09059	.09059
8	-5.476	.4088	.10180	.11830	.11830
9	-6.433	.3959	.10400	.15200	.15200
10	-7.504	.3838	.10590	.19270	.19270
11	-8.705	.3725	.10760	.24150	.24150
12	-10.050	.3620	.10900	.30000	.30000
13	-11.570	.3522	.11030	.36950	.36950
14	-13.260	.3431	.11150	.45170	.45170
15	-15.170	.3347	.11260	.54850	.54850
16	-17.320	.3269	.11370	.66210	.66210
17	-19.740	.3198	.11470	.79480	.79480
18	-22.470	.3133	.11570	.94930	.94930
19	-25.570	.3073	.11680	1.12900	1.12900
20	-29.090	.3020	.11790	1.33600	1.33600
21	-33.130	.2974	.11920	1.57600	1.57600
22	-37.800	.2934	.12060	1.85200	1.85200
23	-43.240	.2902	.12220	2.17000	2.17000
24	-49.660	.2879	.12420	2.53500	2.53500

Note: The particle is injected at an angle of .01 degree with the axis of the accelerator designed in section 4.3.1.

Table 5

Numerical values of the Excursions and $\Delta\dot{r}_{nold}$, $\Delta\dot{z}_{nold}$ and $\Delta E_{nold}/q$ Given by the Equations 4.1, 4.2 and 4.3

N	$\Delta\dot{r}_{nold}$ (Meter/sec)	$\Delta\dot{z}_{n}$ (Km/Sec)	$\Delta E_{nold}/q$ (Mv)	X(N) (cm)	Y(N) (cm)
1	-.416	.4884	.06907	.0	.0
2	-1.155	.4884	.07702	.01006	.01006
3	-1.823	.4784	.08324	.02111	.02111
4	-2.470	.4656	.08842	.03390	.03390
5	-3.135	.4513	.09272	.04923	.04923
6	-3.845	.4367	.09629	.06785	.06785
7	-4.620	.4225	.09930	.09059	.09059
8	-5.478	.4088	.10180	.11830	.11830
9	-6.436	.3959	.10400	.15200	.15200
10	-7.509	.3838	.10590	.19270	.19270
11	-8.714	.3725	.10760	.24160	.24160
12	-10.070	.3620	.10900	.30000	.30000
13	-11.590	.3522	.11030	.36960	.36960
14	-13.300	.3431	.11150	.45180	.45180
15	-15.230	.3347	.11260	.54880	.54880
16	-17.410	.3269	.11360	.66250	.66250
17	-19.880	.3198	.11460	.79540	.79540
18	-22.690	.3133	.11560	.95030	.95030
19	-25.890	.3074	.11670	1.13000	1.13000
20	-29.580	.3021	.11780	1.33900	1.33900
21	-33.870	.2974	.11890	1.58000	1.58000
22	-38.910	.2935	.12030	1.85800	1.85800
23	-44.900	.2904	.12180	2.17900	2.17900
24	-52.1500	.2881	.12370	2.54900	2.54900

Note: The particle is injected at an angle of .01 degree with the axis of the accelerator designed in section 4.3.1.

Chapter 5

CONCLUSION

It has been shown that a Sloan-Lawrence drift tube structure designed for a particle with a fixed nominal charge to mass ratio accepts particles with a wide range of charge to mass ratios, both higher and lower than the nominal value. The range of acceptable charge to mass ratio for a particle injected at certain slope with the axis of the accelerator is largest if the structure contains quadrupole focusing elements. For instance, for a structure with quadrupoles and designed for a charge to mass ratio of 30 Coulombs/Kg, the acceptance range is approximately 26.2 Coulombs/Kg to 83.5 Coulombs/Kg. The exact acceptance range depends upon the particular injection conditions.

The energy gain of a particle in a structure consisting of a given number of drift tube sections depends critically upon the field geometry via the ratio of drift tube radius to section length. For instance, for a 30 drift tube section structure designed for a charge to mass ratio of 30 Coulombs/Kg and operating at 50 KHz, the energy gain of a particle is increased by more than 50% if the drift tube radius is halved from 4 cm to 2 cm.

The inclusion of quadrupoles increases the acceptance for particles which are injected at an angle to the accelerator axis. For a structure designed for a given charge to mass ratio and a fixed quadrupole voltage, the focusing effect of the quadrupoles is best at lower frequencies. For higher frequencies the section lengths and consequently the quadrupole lengths, are shorter, and hence the focusing effect is decreased.

A new set of equations to describe the particle motion in the accelerator has been developed. These equations are more accurate for the off axis and nonsynchronous particles than those equations used by previous workers. For a given accelerator structure and a given set of injection conditions, the two different sets of equations lead to results which differ by as much as 5%.

REFERENCES

1. Kerst, D. W., and Serber, R., Electronic Orbits in the Induction Accelerator, Phys. Rev., Vol. 60, 1941, pp. 53-58.

2. Panofsky, W. K. H., U.C.R.L. 1216 - University of California Radiation Laboratory, Berkeley, California

3. Courant, E. D., Livingston, M. S., and Snyder, H. S., The Strong Focusing Synchroton - A New High Energy Accelerator, Phys. Rev., Vol. 88, 1952, pp. 1190-1194.

4. Blewett, J. P., Radial Focusing in the Linear Accelerator, Phys. Rev., Vol. 88, 1952, pp. 1197-1199.

5. Bell, J. S., A Divided Drift-Tube for Focusing a Proton Linear Accelerator, A.E.R.E. Report No. T/R 1072, 1952, Harwell, England.

6. Teng, L. C., Alternating Gradient Electrostatic Focusing for Linear Accelerators, Rev. Sci. Instr., Vol. 25, 1954, pp. 264-268.

7. Gluckstern, R. L., Focusing in Linear Ion Accelerators, Rev. Sci. Instr., Vol. 26, 1955, pp. 220-228.

8. King, N. M., Proton Dynamics in the Linear Accelerator, II. A/G - Focused Section, 10-50 Mev., A.E.R.E. Report No. T/M 118, 1955, Harwell, England.

9. Courant, E. D. and Snyder, H. S., Theory of the Alternating-Gradient Synchroton, Annuls of Physics :3, 1958, pp. 4-17.

10. Rosenblatt, J., Design of Alternating Gradient Quadrupole Lenses, Nuclear Instruments and Methods 5, 1959, pp. 152-155, North-Holland Publishing Co.

11. Enge, H. A., Ion Focusing Properties of a Quadrupole Lens Pair, Rev. Sci. Instr., Vol. 30, 1959, pp. 248-251.

12. Boussard, D., Focusing in Linear Accelerators, Chapter 5.2, pp. 242, 1966, Institut D'Electronique, Faculté Des Sciences D'Orsay Seine Et Oise, France.

13. Banford, A. P., The Transport of Charged Particle Beams, pp. 35 and 37, First edition, 1966, E. & F. N. Spon Limited, London.

14. Friehmelt, R., Dimensionierung der Quadrupolfokussierung in einem Schwerionen - Linearbeschleuniger, Bericht Nr. 5-67, pp. 9-15, 1967, Institut Für Angewandte Physik Universität Heidelberg, Unilac-Gruppe.

APPENDIX 1

TRANSIT TIME FACTOR

In the Sloan-Lawrence structure the "transit time factor" for a synchronous particle in the n^{th} section is defined as follows:

$$T_{s,n}(r) = \frac{\displaystyle\int_{-LS_n/2}^{LS_n/2} E_Z(r,Z)\ \cos\frac{\pi Z}{LS_n}\ dZ}{\displaystyle\int_{-LS_n/2}^{LS_n/2} E_Z(r,Z)\ dZ} \qquad \text{------------------(A1-1)}$$

In order to compute $T_{s,n}(r)$, $E_Z(r,Z)$ is evaluated subject to the following boundary conditions:

$$\begin{aligned} E_Z(a,Z) &= 0 \qquad \text{for} \quad -LS_n/2<Z<-g_n/2 \ ;\ g_n/2<Z<LS_n/2 \\ &= V_m/g_n \qquad \text{for} \quad -g_n/2<Z<g_n/2 \end{aligned} \qquad \text{------------------(A1-2)}$$

Because the microparticle accelerator operates at a very low frequency, the wave length λ of the electromagnetic field is very much larger than the length of a gap. Hence, retardation times in a gap are negligible and the gap field satisfies Laplace's equation. Thus the scalar potential $V(r,Z)$ in the gap is given by

$\nabla^2 V(r,Z) = 0$

The solution of the above equation is

$V(r,Z) = \left[A\ I_0(pr) + B\ K_0(pr)\right]\left[C\ COS(pZ) + D\ SIN(pZ)\right]$

where A, B, C, D and p are constants and, I_0 and K_0 are the modified Bessel functions of first kind.

Since, V(r,Z) is finite at r=0, B is zero. Thus V(r,Z) becomes

$V(r,Z) = \left[K' COS(pZ) + K'' SIN(pZ)\right]\ I_0(pr)$

where K' and K'' are the new constants.

It is now assumed that the structure is periodic in Z. Although the actual period is approximately LS_n, for the purpose of the computation of the gap fields it is assumed that the periodicity is $(m)(LS_n)$, where m can be taken to be any even integer. The later assumption has little effect on the actual gap field, but it greatly simplifies the computations. Thus, if m is taken as 2, then p in the above equation can be written as

$$p = \frac{K\Pi}{LS_n}$$

where K = 1, 2, -------

The foregoing equation now becomes

$$V(r,Z) = \left\{K' COS\left(\frac{K\Pi Z}{LS_n}\right) + K'' SIN\left(\frac{K\Pi Z}{LS_n}\right)\right\} I_0\left(\frac{K\Pi r}{LS_n}\right) \text{ ----------------- (A1-3)}$$

V(a,Z) as specified by A1-2 is now expanded in a Fourier Series as

$$V(a,Z) = \sum_{K=1}^{\infty}\left\{A_K\ COS\left(\frac{K\Pi Z}{LS_n}\right) + B_K\ SIN\left(\frac{K\Pi Z}{LS_n}\right)\right\}$$

To satisfy the above boundary condition A1-3 is written as

$$V(r,Z) = \sum_{K=1}^{\infty} \left\{ A_K \cos\left(\frac{K\Pi Z}{LS_n}\right) + B_K \sin\left(\frac{K\Pi Z}{LS_n}\right) \right\} \left\{ \frac{I_0\left(\frac{K\Pi r}{LS_n}\right)}{I_0\left(\frac{K\Pi a}{LS_n}\right)} \right\} \text{-----(A1-4)}$$

Since the electrical centre of a gap, Z = 0, is defined as

$$\int_{-LS_n/2}^{LS_n/2} E_Z(r,Z) \sin\left(\frac{\Pi Z}{LS_n}\right) dZ = 0 \text{ -------------------------------(A1-5)}$$

It follows that V(r,Z) is an odd function of Z. Thus A1-4 becomes

$$V(r,Z) = \sum_{K=1}^{\infty} B_K \frac{I_0\left(\frac{K\Pi r}{LS_n}\right)}{I_0\left(\frac{K\Pi a}{LS_n}\right)} \sin\left(\frac{K\Pi Z}{LS_n}\right) \text{ --------------------------(A1-6)}$$

Hence,

$$E_Z(r,Z) = -\frac{\partial V(r,Z)}{\partial Z} = -\sum_{K=1}^{\infty} \left(\frac{K\Pi}{LS_n}\right)(B_K) \frac{I_0\left(\frac{K\Pi r}{LS_n}\right)}{I_0\left(\frac{K\Pi a}{LS_n}\right)} \cos\left(\frac{K\Pi Z}{LS_n}\right)$$

$$\text{------------------------(A1-7)}$$

Substituting A1-7 in A1-1 one obtains

$$T_{s,n} = \frac{\displaystyle\int_{-LS_n/2}^{LS_n/2} -\sum_{K=1}^{\infty} B_K \frac{K\Pi}{LS_n} \frac{I_0\left(\frac{K\Pi r}{LS_n}\right)}{I_0\left(\frac{K\Pi a}{LS_n}\right)} \cos\left(\frac{K\Pi Z}{LS_n}\right) \cos\left(\frac{\Pi Z}{LS_n}\right) dZ}{\displaystyle\int_{-LS_n/2}^{LS_n/2} E_Z(r,Z)\, dZ}$$

Since $B_K = 0$ for K even, one obtains

$$\int_{-LS_n/2}^{LS_n/2} B_K \cos\left(\frac{K\Pi Z}{LS_n}\right) \cos\left(\frac{\Pi Z}{LS_n}\right) dZ = 0 \quad \text{for } K \neq 1$$

Now, assuming that the particle traverses the section at constant r and using the foregoing result, $T_{s,n}(r)$ becomes

$$T_{s,n}(r) = \frac{-(B_1)\dfrac{\Pi}{LS_n} \dfrac{I_0\left(\frac{\Pi r}{LS_n}\right)}{I_0\left(\frac{\Pi a}{LS_n}\right)} \displaystyle\int_{-LS_n/2}^{LS_n/2} \cos^2\left(\frac{\Pi Z}{LS_n}\right) dZ}{V_m}$$

$$= \frac{-(B_1)\left(\dfrac{\Pi}{2}\right) \dfrac{I_0\left(\frac{\Pi r}{LS_n}\right)}{I_0\left(\frac{\Pi a}{LS_n}\right)}}{V_m} \quad \text{-----------------------------(A1-8)}$$

B_1 is found out from the boundary condition A1-2 as follows:

From A1-2 and A1-6 one obtains

$$\int_{-LS_n/2}^{LS_n/2} E_Z(a,Z) \cos\left(\frac{\Pi Z}{LS_n}\right) dZ = \int_{-g_n/2}^{g_n/2} \frac{V_m}{g_n} \cos\left(\frac{\Pi Z}{LS_n}\right) dZ$$

$$= \int_{-LS_n/2}^{LS_n/2} -\sum_{K=1}^{\infty} B_K \left(\frac{K\Pi}{LS_n}\right) \cos\left(\frac{K\Pi Z}{LS_n}\right) dZ$$

Upon integration the last two integrals become

$$\left(\frac{V_m}{g_n}\right)\left(\frac{4\,LS_n}{\Pi}\right)\mathrm{SIN}\left(\frac{\Pi g_n}{2LS_n}\right) = -\,B_1\Pi$$

$$-\,B_1 = \frac{V_m}{\Pi^2}\left(\frac{4LS_n}{g_n}\right)\mathrm{SIN}\left(\frac{\Pi g_n}{2LS_n}\right) \quad \text{-------------------------------(A1-9)}$$

From A1-8 and A1-9 the transit time factor can now be written as

$$T_{s,n}(r) = \frac{\mathrm{SIN}\left(\frac{\Pi g_n}{2LS_n}\right)}{\frac{\Pi g_n}{2LS_n}}\;\frac{I_0\left(\frac{\Pi r}{LS_n}\right)}{I_0\left(\frac{\Pi a}{LS_n}\right)} \quad \text{---------------------------(A1-10)}$$

APPENDIX 2

INTEGRATION OF EQUATIONS 2-7 OF PAGE 9 AND 2-19 OF PAGE 14 TO COMPUTE $\Delta\dot{r}_n$ AND $\Delta\dot{Z}_n$

To perform the integration of equation 2-7 one proceeds as follows: The radial component of the electric field is computed from A1-6 of appendix 1 as

$$E_r(r,Z) = -\frac{\partial V(r,Z)}{\partial r}$$

$$= -\sum_{K=1}^{\infty} (B_K)\left(\frac{K\Pi}{LS_n}\right) \frac{I_1\left(\frac{K\Pi r}{LS_n}\right)}{I_0\left(\frac{K\Pi a}{LS_n}\right)} \mathrm{SIN}\left(\frac{K\Pi Z}{LS_n}\right) \quad \text{--------------(A2-1)}$$

where $I_1\left(\frac{K\Pi r}{LS_n}\right)$ is the modified Bessel function of first order.

Thus, the first integral on the R.H.S. of equation 2-7 can be written as

$$\int_{-LS_n/2}^{LS_n/2} E_r(r,Z)\,\mathrm{SIN}\left(\frac{\Pi Z}{LS_n}\right) dZ = \int_{-LS_n/2}^{LS_n/2} -\sum_{K=1}^{\infty} B_K\left(\frac{K\Pi}{LS_n}\right)\frac{I_1\left(\frac{K\Pi r}{LS_n}\right)}{I_0\left(\frac{K\Pi a}{LS_n}\right)} \mathrm{SIN}\left(\frac{K\Pi Z}{LS_n}\right)\mathrm{SIN}\left(\frac{\Pi Z}{LS_n}\right) dZ$$

Assuming that the particle traverses the gap at constant r the above equation becomes

$$\int_{-LS_n/2}^{LS_n/2} E_r(r,Z)\ \mathrm{SIN}(\frac{\Pi Z}{LS_n})\ dZ = (-B_1)(\frac{\Pi}{2})\ \frac{I_1(\frac{\Pi r}{LS_n})}{I_0(\frac{\Pi a}{LS_n})}$$

Substituting the value of B_1 from A1-9 and using the equation A1-10 the foregoing equation becomes

$$\int_{-LS_n/2}^{LS_n/2} E_r(r,Z)\ \mathrm{SIN}(\Pi Z/LS_n)\ dZ = V_m\ T_{s,n}(0)\ I_1(\Pi r/LS_n) \text{ -------(A2-2)}$$

This can be written as

$$\int_{-LS_n/2}^{LS_n/2} E_r(r,Z)\ \mathrm{SIN}(\Pi Z/LS_n)\ dZ = R\ V_m \text{ ----------------------(A2-3)}$$

where $R = T_{s,n}(0)\ I_1(\Pi r/LS_n)$ ------------------------------(A2-4)

To find the second integral of equation 2-7 one proceeds as follows:

Differentiating both sides of equation A2-3 w.r.t. LS_n one obtains

$$\int_{-LS_n/2}^{LS_n/2} \frac{d}{dLS_n} E_r(r,Z)\ \mathrm{SIN}(\frac{\Pi Z}{LS_n})\ dZ + \frac{1}{2} E_r(r,\frac{LS_n}{2}) - \frac{1}{2} E_r(r,-\frac{LS_n}{2}) = V_m \frac{dR}{dLS_n}$$

where $E_r(r,LS_n/2)$ and $E_r(r,-LS_n/2)$ are the values of E_r at the two limits $Z = \pm LS_n/2$. Since a very little error is introduced in

assuming that the limits of integration $\pm LS_n/2$ can be extended infinitely on both sides, one can assume E_r in the foregoing equation to be zero. Thus the above equation becomes

$$\int_{-LS_n/2}^{LS_n/2} \frac{d}{dLS_n}\left\{E_r(r,Z)\ \mathrm{SIN}(\Pi Z/LS_n)\right\} dZ = V_m \frac{dR}{dLS_n}$$

Upon differentiation one obtains

$$\int_{-LS_n/2}^{LS_n/2} (\Pi Z/LS_n)\ E_r(r,Z)\ \mathrm{COS}(\Pi Z/LS_n)\ dZ = -V_m\ LS_n \frac{dR}{dLS_n} \text{ -------(A2-5)}$$

$\frac{dR}{dLS_n}$ of A2-4 is given by

$$\frac{dR}{dLS_n} = -\frac{\Pi}{LS_n^2}\left[\frac{\mathrm{SIN}(\frac{\Pi g_n}{2LS_n})}{(\frac{\Pi g_n}{2LS_n})}\left\{\frac{I_0(\frac{\Pi a}{LS_n})}{(\frac{\Pi}{LS_n})}\left[I_1(\Pi r/LS_n) + \frac{\Pi r}{LS_n} I_2(\frac{\Pi r}{LS_n})\right] - a\, I_1(\frac{\Pi r}{LS_n})\, I_1(\frac{\Pi a}{LS_n})\right\} + \frac{I_1(\frac{\Pi r}{LS_n})}{I_0(\frac{\Pi a}{LS_n})}\left\{\frac{\frac{\Pi}{LS_n}\cdot(\frac{g_n}{2})^2\ \mathrm{COS}(\frac{\Pi g_n}{2LS_n}) - \frac{g_n}{2}\ \mathrm{SIN}(\frac{\Pi g_n}{2LS_n})}{(\frac{\Pi g_n}{2LS_n})^2}\right\}\right]$$

----------------------(A2-6)

To find the integral of equation 2-19 one can write the equation A1-1 of appendix 1 as

$$\int_{-LS_n/2}^{LS_n/2} E_Z(r,Z)\, \mathrm{COS}(\Pi Z/LS_n)\, dZ = V_m\, T_{s,n}(r) \quad \text{------------------(A2-7)}$$

where $T_{s,n}(r)$ is given by A1-10 of appendix 1.

Now, differentiating both sides of A2-6 w.r.t. LS_n one obtains

$$\int_{-LS_n/2}^{LS_n/2} (\Pi Z/LS_n)\, E_Z(r,Z)\, \mathrm{SIN}(\Pi Z/LS_n)\, dZ = -\, LS_n\, V_m \frac{dT_{s,n}(r)}{dLS_n}$$

$$\text{---------------(A2-8)}$$

where $\dfrac{dT_{s,n}}{dLS_n}$ is given by

$$\frac{dT_{s,n}}{dLS_n} = -\frac{\Pi}{LS_n^2}\left[\frac{\mathrm{SIN}\left(\frac{\Pi g_n}{2LS_n}\right)}{\left(\frac{\Pi g_n}{2LS_n}\right)}\left\{\frac{r\, I_0\left(\frac{\Pi a}{LS_n}\right) I_1\left(\frac{\Pi r}{LS_n}\right) - a\, I_0\left(\frac{\Pi r}{LS_n}\right) I_1\left(\frac{\Pi a}{LS_n}\right)}{\left\{I_0\left(\frac{\Pi a}{LS_n}\right)\right\}^2}\right\}\right.$$

$$\left. + \frac{I_0\left(\frac{\Pi r}{LS_n}\right)}{I_0\left(\frac{\Pi a}{LS_n}\right)}\left\{\frac{\frac{\Pi}{LS_n}\left(\frac{g_n}{2}\right)^2 \mathrm{COS}(\Pi g_n/2LS_n) - (g_n/2)\, \mathrm{SIN}(\Pi g_n/2LS_n)}{(\Pi g_n/2LS_n)^2}\right\}\right]$$

$$\text{----------------------(A2-9)}$$

APPENDIX 3

PHASE OSCILLATION

The synchronous phase changes by 2Π in going from one section to the next. The change in phase for a nonsynchronous particle moving from the n^{th} to the $(n+1)^{th}$ section with velocity v_n is given by

$$\Pi + \omega t_n = \Pi + \frac{2\Pi\, LS_n(1+k_n)}{T_\circ v_{s,n}} = \Pi\,(2+k_n) \text{ -------------------(A3-1)}$$

The nonsynchronous phase at the centre of the n^{th} section is

$$\phi_n = \phi_o + \sum_{p=1}^{n} \Pi(2+k_p) \text{ --(A3-2)}$$

where ϕ_o is the phase of the electric field at the instant the nonsynchronous particle is injected.

The synchronous phase at the centre of the n^{th} section is given by

$$\phi_{s,n} = \phi_s + 2n\Pi$$

where ϕ_s is the phase of the electric field at the instant the synchronous particle is injected. Thus, the oscillation of nonsynchronous phase about the synchronous phase is

$$\Delta\phi_n = \phi_n - \phi_{s,n}$$

$$= (\phi_o - \phi_s) + \Pi \left\{ \sum_{p=1}^{n} (2 + k_p) - 2n \right\} \text{ ------------------(A3-4)}$$

[illegible]